

DR. KARL REMEIS-STERNWARTE
FRIEDRICH-ALEXANDER-UNIVERSITÄT
ERLANGEN-NÜRNBERG

Bachelorarbeit aus der Physik

X-Ray Study of the Fornax Dwarf Spheroidal Galaxy

Vorgelegt von
Martin Reh
15. Februar 2023



Betreuerin: Prof. Dr. Manami Sasaki

Contents

1	Theory	3
1.1	Dwarf Galaxies	3
1.2	The Fornax Dwarf Galaxy	4
1.3	eROSITA	5
2	Data Analysis	8
2.1	Data Calibration and Source Detection	8
2.2	Preparation of the Catalog	11
2.2.1	Astrometric Calibration	11
2.2.2	Sorting and Filtering the Catalog	12
2.3	Source Matching and Classification	13
2.3.1	Source Matching	13
2.3.2	Isochrones	19
2.3.3	Further Classification and Source Properties	22
2.3.4	Unclassified Sources	28
2.4	Comparison to XMM-Study	31
2.5	The Globular Clusters of Fornax	33
3	Conclusion	36
4	Acknowledgements	41
5	Appendix	42
6	Eigenständigkeitserklärung	52

1 Theory

This chapter is dedicated to provide useful background information concerning the eROSITA mission and dwarf galaxies in general, as well as interesting features and properties of the Fornax dwarf spheroidal galaxy (Fornax dSph in the following) in particular.

1.1 Dwarf Galaxies

In general dwarf galaxies are regarded as smaller versions of normal galaxies, typically defined by their mass or the number of stars that they contain. These galaxies only have around 1000 or up to a couple billion stars. The Milky Way as a reference has around 60 billion stars in it (Licquia and Newman, 2015). Dwarf galaxies are one of the most common types of galaxies in the universe. These galaxies often form groups with normal galaxies and are typically thought to be gravitationally bound to their host galaxy. However, this assumption has been difficult to maintain lately, since the 3D velocities of most of the dwarf galaxies have been measured to be much higher than expected. This as a consequence would mean that most of these galaxies are interacting with the Milky Way for the first time, because their energies are too high to maintain a galactic orbit (Hammer et al., 2021). Meaning, they did not orbit the Milky Way before and therefore come in contact with it for the first time. In the case of our Milky Way, there are around 50 known dwarf galaxies surrounding it, though most of them are pretty small. The most massive ones in our galactic neighborhood are the Large Magellanic Cloud (LMC) and the Small Magellanic Cloud (SMC). Both of them can be seen by the naked eye from the southern hemisphere of the earth. The smaller dwarf galaxies are usually named after the constellation, in which they appear (ESA, 2021b). Figure 1 shows Gaia data of the most massive dwarf galaxies surrounding the Milky Way.

Dwarf galaxies, like normal galaxies, also come in a huge variety of shapes and sizes. Like normal galaxies they are also classified into types like spiral, elliptical, irregular or spheroidal dwarf galaxies. Because they have fewer stars compared to the larger galaxies and also fewer gas, dwarf galaxies are usually much fainter. Nevertheless dwarf galaxies are interesting objects to study because they could provide insight into the early universe. Furthermore, they usually contain a high amount of dark matter, which could also help in solving the mystery of it (ESA/Hubble, c).

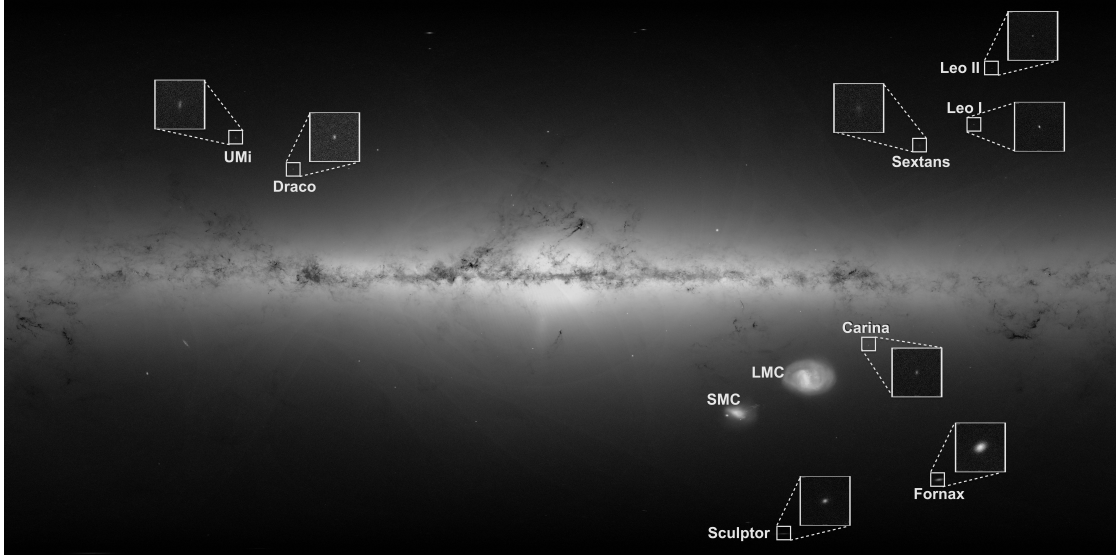


Figure 1: Gaia EDR3 Data showing some of the dwarf companion galaxies of the Milky Way (ESA, 2021a).

1.2 The Fornax Dwarf Galaxy

The Fornax dwarf galaxy is a satellite galaxy of the Milky Way and can be found in the constellation of Fornax. It is located at a right ascension of 02:39:59.00 and a declination of $-34:27:00.00$ (Mateo, 1998), is 138 ± 8 kpc away (de Boer et al., 2012), determined using RR Lyrae stars and it has a semi-major axis of 17 arcmin and a semi-minor axis of 13 arcmin, as well as a position angle of 48° (Nucita, A. A. et al., 2013). Furthermore, it is the brightest spheroidal dwarf galaxy in the group of the Milky Way with an absolute magnitude of $M_V = -13.2$ mag (Mateo, 1998). An optical picture of the galaxy can be seen in Figure 2. It was found by Harlow Shapley in 1938 on a photographic plate, which is quite late in comparison to other galaxies (Shapley, 1938). This is most likely due to a very low apparent magnitude of only 9.3 mag although it is the brightest dwarf spheroidal. As a result the galaxy was only found photographically, because it is too dim to see with the naked eye. Furthermore, the galaxy is host to five globular clusters, some of which were already discovered before the galaxy itself. Some of the clusters are shown in Figure 3 in detailed Hubble images. Such a high number of globular clusters for a galaxy of this small size is quite rare. As a result the galaxy has already been studied quite a bit. According to a range of N-body simulations carried out by Cole et al. (2012) these clusters are only sustainable with a large dark-matter core. Otherwise they would be pulled into the galaxy by dynamical friction.

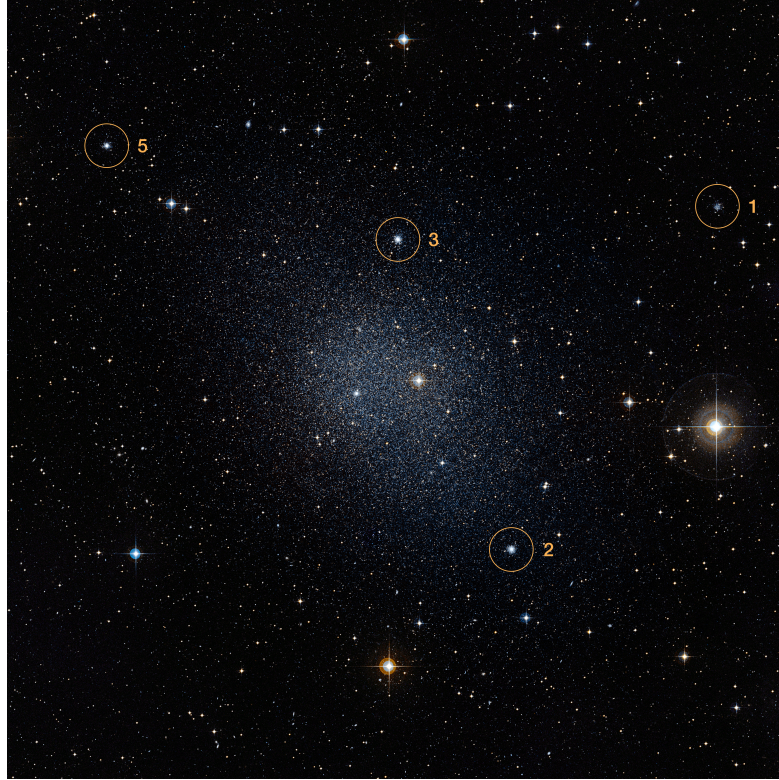


Figure 2: Digitized Sky Survey 2 image of the Fornax dSph with four of its globular clusters marked (ESA/Hubble, a).

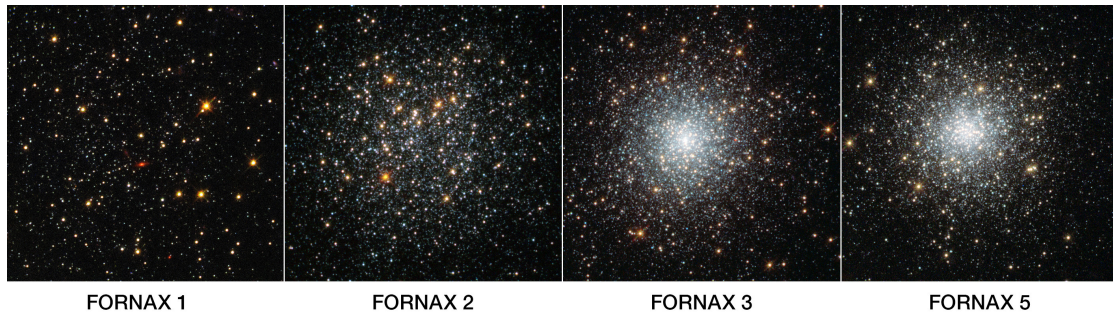


Figure 3: Hubble images of globular clusters 1, 2, 3 and 5 of the Fornax dSph (ESA/Hubble, b).

1.3 eROSITA

eROSITA (extended Roentgen Survey with an Imaging Telescope Array) is an X-ray telescope under the lead of the Max Planck Institute for Extraterrestrial Physics in Germany. It is part of a collaboration between Russia and Germany and is installed

on board of the Spektr-RG as its host spacecraft. Alongside eROSITA the Spektr-RG also carries the russian telescope ART-XC (Astronomical Roentgen Telescope X-ray Concentrator), which is also a X-Ray telescope, but more sensitive towards higher energies than eROSITA. The mission was successfully launched on July 13, 2019 from the Baikonur cosmodrome in Kazakhstan. It is currently in a halo orbit around L2. As this is an instable orbit, corrections are necessary so that the spacecraft does not drift off over time. The eROSITA telescope was specifically designed to observe large areas of the sky with great detail and high sensitivity and the goal of the mission was to complete a total of eight All-Sky Surveys until the end of 2023, which are called eRASS1 to eRASS8. When the mission is finished it will provide an up to 25 times more sensitive All-Sky Survey than ROSAT in the soft X-Ray band of 0.2-2.3 keV and the first All-Sky Survey in the hard X-Ray band of 2.3-8 keV. In combination with the second telescope, ART-XC, energies of up to 30 keV can be observed. As estimated by many independent studies eROSITA could detect about 100 000 new galaxy clusters and a few millions of Active Galactic Nuclei (AGNs) alongside many other new X-Ray sources (Predehl, P. et al., 2021).

The general structure of the instrument can be seen in Figure 4. It is made out of seven independent telescope assemblies, ordered in a hexagonal shape, which are shown on the right side of Figure 5 alongside the camera assembly at the back of the telescope. Each of the seven modules has its own Wolter-I type mirror setup and camera and all the modules are aligned to one another. All of the telescope assemblies have a focal length of 1 600 mm and a resolution of 16.1" at 1.5 keV. Since the resolution of the Wolter-I type mirrors degrades rapidly off-axis, the cameras are tilted with regard to one another in order to compensate the off-axis blurring in a later averaged field. This results in an overall averaged resolution of 26" (Predehl, P. et al., 2021).

At the time of this thesis eRASS1 to eRASS4 are accessible and will also be used here. Unfortunately, since February 26, 2022 the operation of the instrument has been paused due to the Russian invasion of Ukraine.

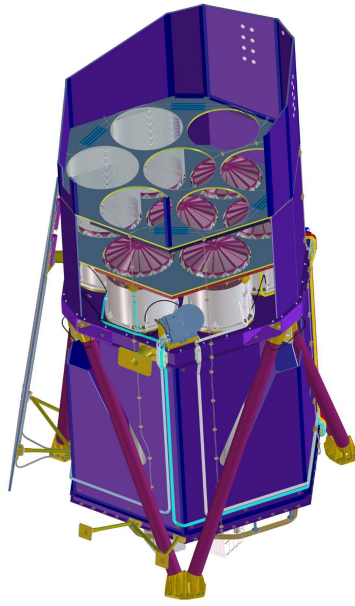


Figure 4: A schematic of the eROSITA telescope. The ART-XC and the spacecraft cannot be seen in this picture (Uni Tuebingen, Eva Laplace, Inga Saathoff, Chris Tenzer, 2018).

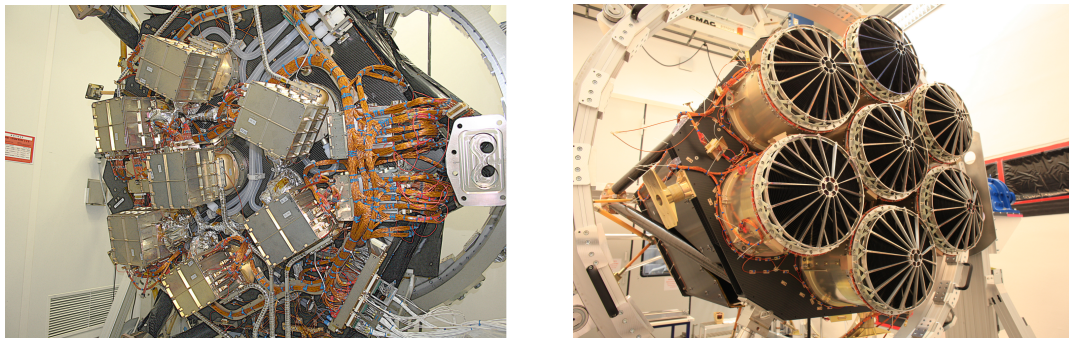


Figure 5: Pictures of the eROSITA telescope in assembly. On the right side the Wolter mirrors can be seen and on the left side the seven cameras at the back of the optical assembly of the telescope (Predehl, P. et al., 2021).

2 Data Analysis

In this chapter the data of the four all sky surveys of eROSITA, called eRASS1 to eRASS4, are used to analyse the Fornax dSph. Since the dataset is organized in different tiles and the galaxy lies on the border of those, three tiles were used in order to cover the whole galaxy. The dataset was analysed using the eROSITA Science Analysis Software System (eSASS) and later on also with provided python scripts and self written code. The first goal was to make an image and catalogs out of the raw event files for all of the eRASS observations. Furthermore, a combined dataset of all eRASS observations was created in order to increase the exposure time and potentially detect fainter sources. The goal with these datasets is to look at and identify all the detected sources inside an ellipse centered on the galaxy with a major axis of 85 arcmin and a minor axis of 65 arcmin, which corresponds to 5 times the tidal radius of the galaxy. In order to do that, the sources are matched to different catalogs of VizieR ¹ with the help of a provided python script called Artemis. After establishing different source classes and cross matching the different catalogs, the nature of the sources and also possible Fornax candidates can be shown. As the Fornax dSph is dominated by intermediate aged stars (1-10 Gyr populations) and has only little amounts of star forming regions (de Boer et al., 2012), we expect to find very few X-Ray sources in the galaxy. X-Ray sources located in the galaxy may likely be binary systems with only a moderate probability for younger stars. As the galaxy has a strong metallicity gradient from the center to the outer regions (de Boer et al., 2012), these younger stars are mainly expected near the center of the galaxy or maybe even in the globular clusters. Additionally, possible sources located in the five globular clusters of Fornax could be quite interesting, and will therefore be examined more closely later on. Moreover the detected eROSITA sources will also be cross-matched and compared to another XMM-Newton study of the dwarf galaxy (Nucita, A. A. et al., 2013). This XMM-study is expected to detect more sources, as it has around 10 ks of exposure time, so around ten times the exposure time of the eROSITA data, but a much more narrow field of view. The XMM-Newton data therefore do for example not include all the globular clusters.

2.1 Data Calibration and Source Detection

The four eRASS surveys were captured starting on December 13, 2019 and completed in the end of 2021. The exposure time of eROSITA varies widely, depending on the region of interest in the sky. The way in which eROSITA observes the sky, results in higher exposure times near the ecliptic poles of around 10 000 s and around 100 s near the ecliptic equator, when looking at a single eRASS observation (Predehl, P. et al., 2021). Since the Fornax dSph is not located around a ecliptic pole the exposure time of each of the observations is near the lower end of the range given above. The effective exposure time for the combined observation ranges from 700 s to around 1000 s.

In order to work with the dataset, the eROSITA Science Analysis Software System

¹ <https://vizier.cds.unistra.fr/viz-bin/VizieR>

(eSASS) was used, which is an accumulation of different tools from the Max Planck Institute for Extraterrestrial Physics. It is used in order to calibrate the dataset, create images in different energy bands, detect sources, do spectral analysis and organize all the found sources into a catalog. To take a first look at the data, a couple of images were created with the image tool of eSASS (evtool). Figure 6 shows the full energy range from 0.2 keV to 10 keV of all the eRASS observations combined and Figure 7 shows a RGB image with different energy bands in the different color channels. For the red channel energy band 1 was used, for the green channel band 2 and for the blue channel band 3. The source detection was executed on every single eRASS as well as the combined one, according to the eROSITA cookbook ². Three image tiles were used in order to display the whole galaxy. For the images the data was rebinned at a rebin size of 80 at an image size of 3240. The used energy bands for the source detection can be seen in Table 1. The energy bands are the standard energy bands of eROSITA, but the second band, which normally runs from 0.6 keV to 2.3 keV was split up into two bands, in order to have an improved accuracy for soft X-Ray sources when later analysing the data.

Band	Energy Range [keV]
Band 1	0.2 - 0.6
Band 2	0.6 - 1.1
Band 3	1.1 - 2.3
Band 4	2.3 - 5.0

Table 1: The energy bands selected in the eSASS scripts, which will be used later on in the thesis.

With the use of eSASS, exposure maps and also background maps were created. After calibration, the exposure maps already account for the sensitivity variation and vignetting of the detector.

In total, 3891 sources were found in the three image tiles when combining all the observations. The number of sources for each single observation can be seen in Table 2.

² <https://erosita.mpe.mpg.de/edr/DataAnalysis/esasscookbook.html>

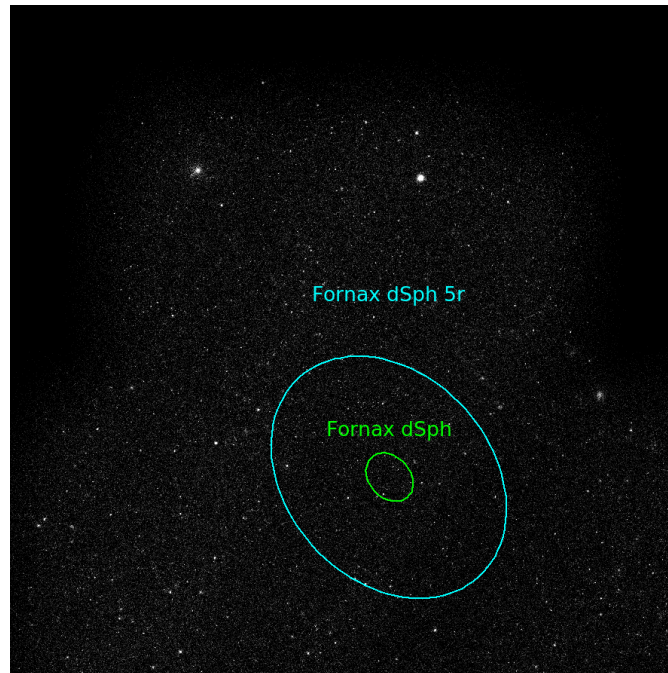


Figure 6: Grayscale image of the combined observations in the energy range of 0.2 keV to 10 keV. The green and cyan ellipses show the tidal radius of Fornax (17 arcmin) and the analysis region with five times the semi-major axis (85 arcmin), respectively.

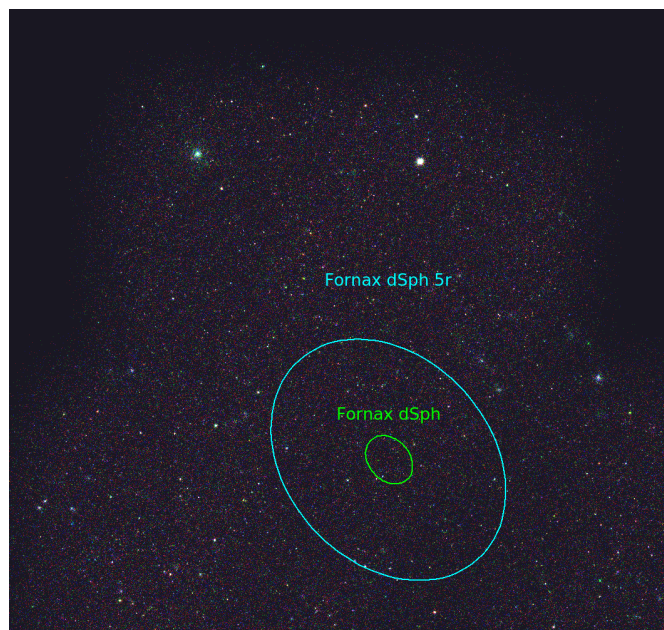


Figure 7: RGB image with the data of the combined observations. R image corresponds to energy band 1, G to energy band 2 and B to energy band 3. The green and cyan ellipses show the tidal radius of Fornax (17 arcmin) and the analysis region with five times the semi-major axis (85 arcmin), respectively.

Observation	Number of detected sources
eRASS1	413
eRASS2	469
eRASS3	306
eRASS4	389
Combined	3891

Table 2: The number of detected sources with the eSASS scripts for each observation and the combination of all the observations.

After running the source detection, a catalog of the found sources was created for each observation and the combined one, which was also done by the eSASS scripts. This catalog now contains all the sources with corresponding source IDs, coordinates of the sources, counts and already calculated hardness ratios, and all the corresponding errors.

2.2 Preparation of the Catalog

2.2.1 Astrometric Calibration

After creating the catalogs for each observation, the coordinates of the detected sources need to be verified and also corrected with other catalogs in order to achieve higher

pointing accuracy. By crossmatching other catalogs to the sources found by eROSITA, the positional differences of the sources can be calculated and later on used to calibrate the eROSITA data. This should result in more accurate coordinates than those, which can be achieved natively with eROSITA, because of the low count rate of eROSITA compared to other optical or infrared observations for example with GAIA or WISE. To do this a python script called Artemis is used. This script was written by Jonathan Knies of the Dr. Karl Remeis Observatory Bamberg according to an algorithm presented in the paper of Salvato et al. (2017). The script uses online Vizier (Université de Strasbourg/CNRS) catalog data in order to cross-match the eROSITA sources with catalogs given to the script.

To perform the astrometric calibration, all the X-Ray sources were cross-matched with the Gaia-WISE Extragalactic Astrometric Catalog (Paine et al., 2018) and the Million Quasars (Milliquas) Catalog (Flesch, 2021). These catalogs include only background sources like Active Galactic Nuclei (AGNs) and should have better pointing accuracy than the eROSITA sources. It makes sense to calibrate on these AGNs, because these objects are quite abundant, as all of them should be seen in the X-Ray part of the spectrum. This way, 625 sources could be matched with a match probability of over 70% over all the three image tiles. With those matched sources a weighted average positional error could now be calculated over the whole image according to Equation 1.

$$\bar{D} = \frac{\sum_{i=1}^n \omega_i D_i}{\sum_{i=1}^n \omega_i} \quad (1)$$

With D corresponding either to the RA or Dec difference between the eROSITA and the match coordinates, n the number of the matched sources and ω_i the inverse of the eROSITA coordinate error as a weight for the difference. The resulting differences can be seen in Table 3.

Axis	Difference [arcsec]
RA	1.084772
DEC	-0.202140

Table 3: The weighted average distance between the eROSITA coordinates and the matched infrared or optical counterparts.

The calculated difference between the matches and the X-Ray sources was applied to the entire data set, resulting in a new, now corrected eROSITA catalog.

2.2.2 Sorting and Filtering the Catalog

When working with the sources later on, it is important to have reproducible source IDs. To achieve that, all the sources in the catalog were sorted by ascending Right Ascension and were given new source IDs starting at 1. Additionally, since only the sources near the galaxy should be examined, a new catalog was created. This catalog is a filtered version of the catalog worked with up until now. It contains only the sources inside an ellipse

centered on the Fornax dSph with a semi-major axis of 85 arcmin and a semi-minor axis of 65 arcmin and a position angle of 48° , so it corresponds to five times the semi-major and semi-minor axes of the galaxy. This ellipse can also be seen in Figure 7 and Figure 6. The new catalog now includes a total of 411 sources, when using all the observations combined.

2.3 Source Matching and Classification

Now, that the source catalog is complete, the sources can be matched to different catalogs. In particular they will be matched to the the optical GAIA Data Release 2 (DR2) (Gaia Collaboration, 2018), the Wide-field Infrared Survey Explorer (WISE) (Wright et al., 2010) and the Two Micron All Sky Survey (2MASS) (Skrutskie et al., 2006). Both the WISE and the 2MASS catalogs are infrared catalogs and the catalog of Gaia is an optical one.

The bands of Gaia that will be used in the analysis, are the G-band (330-1050 nm) and the blue and red prismphotometer bands G_{BP} (330-680 nm) and G_{RP} (630-1050 nm) respectively. The used bands of 2MASS were the J-band at $1.25 \mu\text{m}$ and the K_s band at $2.16 \mu\text{m}$. And lastly the used bands of WISE were W1 at $3.4 \mu\text{m}$, W2 at $4.6 \mu\text{m}$ and W3 at $12 \mu\text{m}$.

Matching the X-Ray sources with different catalogs especially in other wavelengths is a crucial step in a population study and gives much more data for all the sources and also makes it easier to later classify them.

2.3.1 Source Matching

In the first part, the sources were cross-matched to the WISE catalog. Matching with the WISE catalog first makes sense, because it is possible to sort all the matches in broad categories, which can be analysed further later on. These categories will serve as a kind of basis classification for the rest of the thesis. Only the sources which have a match probability, given by the ARTEMIS script, of over 60% were selected as WISE matches. To determine the different source categories, the matches of the WISE catalog are plotted in a color-color diagram, which can be seen in Figure 9. As Wright et al. (2010) discussed in their paper, the sources in the color-color diagram build up different groups depending on the nature of the source. For example, foreground objects like stars appear near zero color in the color-color diagram, whereas background sources like Active Galactic Nuclei (AGNs) are fainter and redder in W2-W3. This makes it possible to split the plot into different regions, likely corresponding to one source type. The criteria that were used to do this can be seen in Table 4. The regions described in the paper can be seen in Figure 8. As there are not that many sources to distinguish between the smaller subcategories, it makes sense in this case to combine the categories into bigger ones and work with those instead. The three groups that will be used are Stellar Object Candidates, Normal Galaxy Candidates and AGN Candidates. The elliptical and spiral galaxies shown in Figure 8 are combined to the Normal Galaxy Candidates group, stars are considered in the Stellar Object Candidates group and everything fainter or more red

than the Normal Galaxy Candidates would be part of the AGN Candidates group.

Source Type	W1 - W2 [mag]	W2 - W3 [mag]
AGN Candidates	>0.7	>1
Normal Galaxy Candidates	<0.7	>1
Stellar Object Candidates		<1

Table 4: Selection criteria of the source classes in the WISE color-color diagram according to Wright et al. (2010).

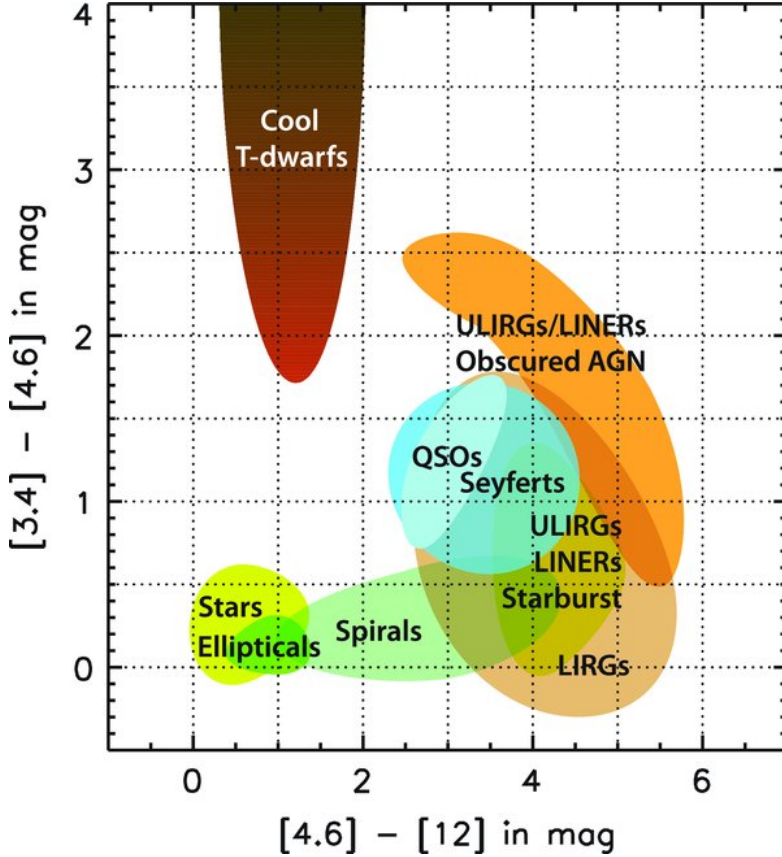


Figure 8: Plot of the different source group regions in the color-color diagram for the WISE data from Wright et al. (2010).

For some sources, there were no error data in the online catalog, in which case only an upper limit was given. These sources were not included in the categories and were marked as *Unclassified Sources*. The results of the source matching with the WISE catalog can be seen in Figure 9. Of the 411 sources included in the catalog, 6 did not have a WISE match at all. Out of the other sources, 251 reached the desired match probability and 160 did not. The 160 sources, which did not reach the match probability, are thus not

included in the color-color diagram. There were 20 Stellar Object Candidates, 123 AGN Candidates, 44 Normal Galaxy Candidates and 64 unclassified sources.

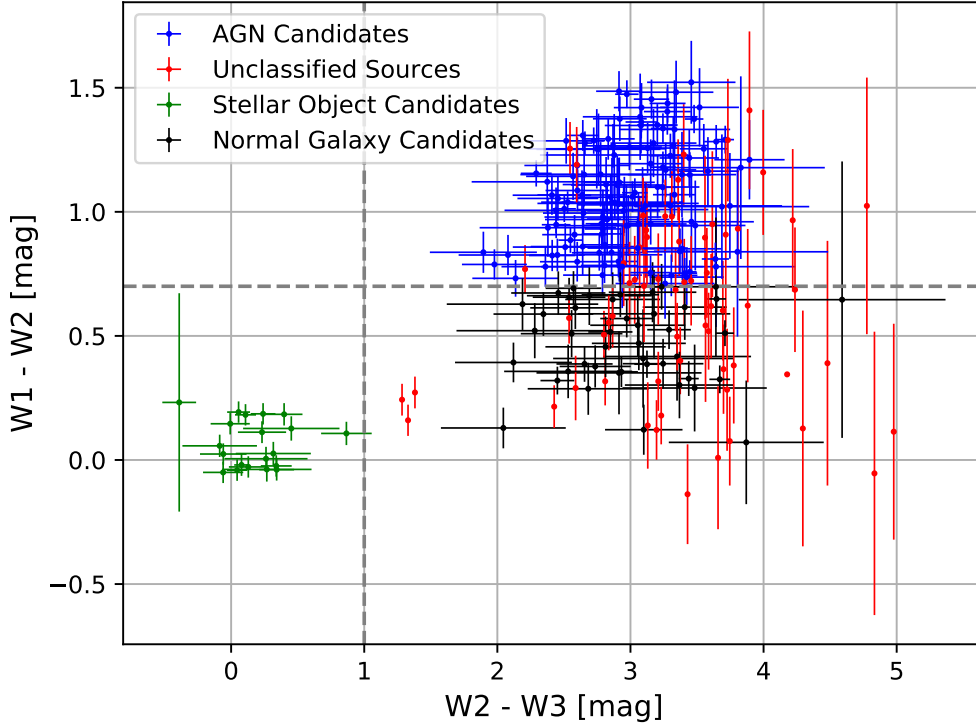


Figure 9: Wise color-color diagram used for the classification of the sources. The grey lines mark the edges of the source group regions according to (Wright et al., 2010).

As expected, most of the sources fall in the Active Galactic Nuclei (AGN) Candidates and Normal Galaxy Candidates category. This is a result of two factors. Firstly, the Fornax dSph is located at a galactic latitude of around -65.7° , thus the amount of foreground stars expected in the field is quite low. This is because at this latitude the dwarf galaxy is far away from the galactic disk, where the star density is much lower. Secondly, with the exposure time of approximately 1 ks one can assume that some of the dimmer sources in the galaxy did not get captured in the data set.

Since the sources in the Fornax dSph are much more distant than objects located in the Milky Way, those sources should appear dimmer and can thus likely be found in the Normal Galaxy Candidates category. The 20 Stellar Object Candidates, that were found, are most likely foreground stars. As such, they should be part of the Milky Way, which will be further discussed in the Isochrones Section.

To get a better idea of the source distribution, another plot was also created, containing all the WISE catalog sources in the region of the galaxy. This plot can be seen in Figure 10.

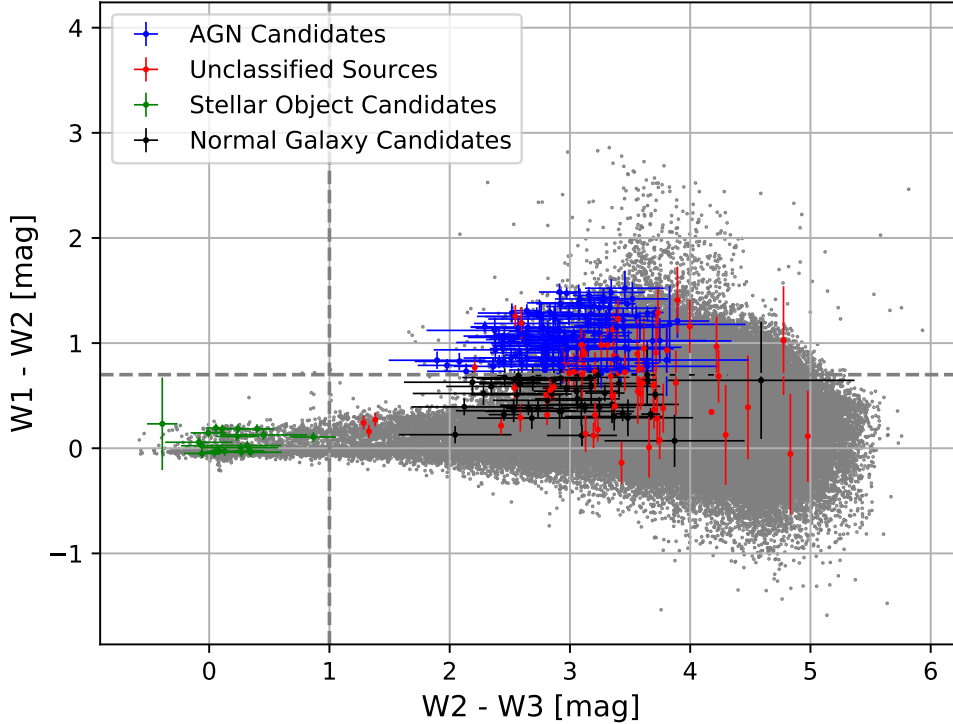


Figure 10: Wise color-color diagram including all WISE catalog sources marked as the grey dots.

With this new plot the aforementioned expectation of seeing mostly AGNs in the region of the galaxy can be confirmed. Also with the catalog data the group of the ULIRGs/LINERs from Figure 8 can now be identified, but no source of the eROSITA data lies in this region. This is also true for the cool T-dwarfs, which is why this group is not used in the later analysis.

In the next step the source data can now be matched with the Gaia and 2MASS catalogs. Matching with the Gaia DR2 catalog resulted in 314 matches, but 118 matches were not included due to lacking match probability, resulting in a total of 196 Gaia matches. Furthermore, also foreground extinction due to our own galaxy will be accounted for in the Gaia data. This will be done in a similar way as in Sestito et al. (2019). For this correction, every Gaia band gets its own individual correction factor as described in Marigo et al. (2008). Based on this information all sources except the Stellar Object

Candidates, as they should not be as effected by the glactic extinction, are de-reddened according to Equation 2 to Equation 4.

$$G_0 = G - 2.664E(B - V) \quad (2)$$

$$BP_0 = BP - 3.311E(B - V) \quad (3)$$

$$RP_0 = RP - 2.021E(B - V) \quad (4)$$

To apply these equations to the data set, a value for $E(B - V)$ of 0.03 according to Mateo (1998) was used. After de-reddening all the sources, these matches again were plotted in a color-magnitude diagram. For Gaia this is usually done by plotting the magnitude of each source in the G-band against the difference in BP and RP magnitudes. The resulting plot is displayed in Figure 11. Since the plot only relies on the Gaia data, some new sources can be seen in the plot as well, which did not have a WISE match. These sources are not classified yet and thus are marked with 'Unclassified Sources' in the plot.

Most of the sources in the Gaia color-magnitude diagram are located on the lower left side of the plot. These sources are, with a G-band magnitude of around 20, quite faint. As expected almost all of them are AGN Candidates and Normal Galaxy Candidates. When taking a closer look, we can again see a grouping of sources. Especially the Stellar Object Candidates are clearly separated from the Normal Galaxy Candidates/AGN Candidates as they are quite bright in the G-band. But also a slight grouping can be observed between the Normal Galaxy Candidates and the AGN Candidates. The Normal Galaxy Candidates seem to be shifted a bit to higher BP-RP values in reference to the AGN Candidates. Furthermore two of the Stellar Object Candidates are very faint with a G-band magnitude of around 21 and thus lie in the AGN Candidates/Normal Galaxy Candidates region. These sources will be discussed further in the Isochrones Section.

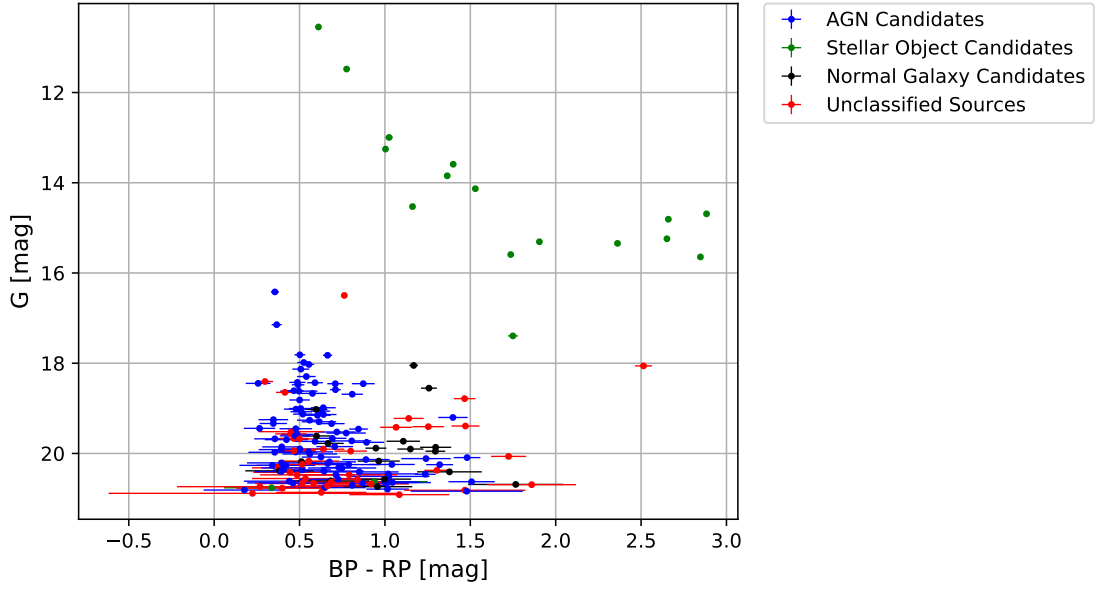


Figure 11: Gaia color magnitude diagram. As in the WISE color-color diagram, the grey dots indicate all the known sources in the region of interest and the colored dots represent the eROSITA sources.

For the 2MASS catalog the script detected 103 matches and after considering the match probability, in total 59 source matches can be used in the data analysis. These sources, like for the other catalogs, were again plotted in a color-magnitude diagram. For 2MASS the K-band magnitude is plotted against the difference in the J- and K-band magnitudes. The resulting plot can be seen in Figure 12. Like in the Gaia color-magnitude diagram, the Normal Galaxy Candidates and AGN Candidates are quite faint and can thus be seen at the bottom of the plot. Again as in the previous plots, source groups are formed. The Stellar Object Candidates are clearly separated from the other candidates, but the 2MASS data did not get enough matches to see if the groups of the AGN Candidates and the Normal Galaxy Candidates can be distinguished. Besides some of the extra unclassified sources are quite bright and seem to fit into the group of the Stellar Object Candidates, these will be discussed in the section of the Unclassified Sources.

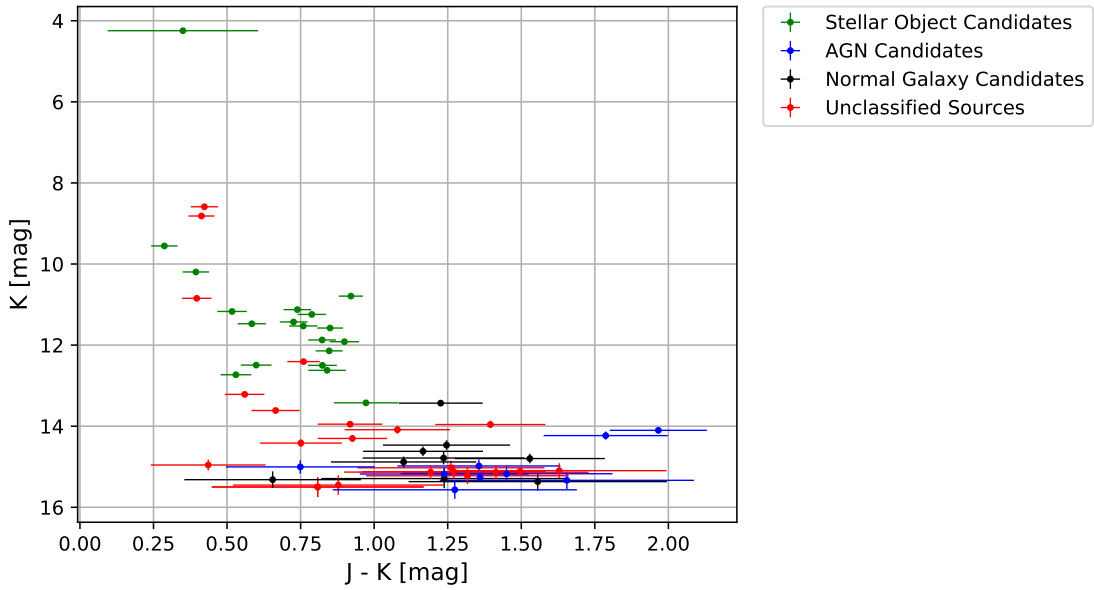


Figure 12: 2MASS color magnitude diagram. The grey dots again indicate all the known sources in the region of interest and the colored sources represent the eROSITA data.

2.3.2 Isochrones

In order to differentiate further between the background sources and stellar foreground population as well as possible Fornax dSph sources, isochrones can be plotted in the diagrams. Isochrones are lines in Hertzsprung-Russel or color-magnitude diagrams, which correspond to groups of stars with the same age, but different masses. The isochrones that are plotted in the diagrams depend on the distance of the sources, the metallicity and the age of the source group. Therefore, conclusions regarding those factors can be drawn from the isochrones. The isochrones needed to be generated for each catalog separately via the online Isochrone and LF Generator³ by the Dartmouth Stellar Evolution Program (DSEP).

In general, there are two goals, which should be achieved with the isochrones. Firstly, we want to map the stellar foreground population in order to confirm the Stellar Object Candidates and secondly we want to trace the stellar evolution of the Fornax dSph in particular to see if there are any obvious sources corresponding to it or not. The first part was to get an idea of the foreground population. To achieve this, three isochrones were plotted in each of the diagrams of Gaia and 2MASS. These are called Galactic isochrones in the plots seen in Figure 13 for Gaia and in Figure 14 for 2MASS. The isochrones were plotted with a metallicity ($[Fe/H]$) of 0 dex, corresponding to the solar metallicity. This is based on the assumption, that the foreground stars are related to the sun's metallicity.

³ http://stellar.dartmouth.edu/models/isolf_new.html

An age of 7 Gyr was used with this isochrone, as it lies more in a middle ground of the stellar age values of the Milky Way. To see how bright/faint the stellar sources get with varying distance, the isochrone was plotted three times for a distance of 100 pc, 200 pc and 300 pc.

Additionally, in both of the plots, all the known catalog sources in the region of the galaxy were plotted as grey dots, like in the WISE color-color diagram. These additional sources help to see the general structures in the color-magnitude diagrams. In the second part the isochrones are used to model the stellar population of the Fornax dSph. According to de Boer et al. (2012) the main part of the stellar population in the dwarf galaxy is around 4 Gyr old and has a metallicity of around -1.0 dex, thus the first three isochrones plotted in Figure 13 are for 4 Gyr, -1.0 dex and for a distance of 128 kpc, 138 kpc and 148 kpc, varying the distance around the measured value of 138 kpc in order to get a feeling for the influence of uncertainties due to the distance measurement on the isochrones. To also account for the older stellar population that de Boer et al. (2012) mentions, another three isochrones were plotted for 10 Gyr and the same metallicity as well as the same distances. For reference also three isochrones were plotted for an age of 1 Gyr, the three distances and a metallicity of -1.0 dex. To visualize the changes in metallicity, another two isochrones were plotted in Figure 13 for the main stellar population at 4 Gyr, the assumed distance of 138 kpc and metallicities of -1.5 dex and -0.75 dex.

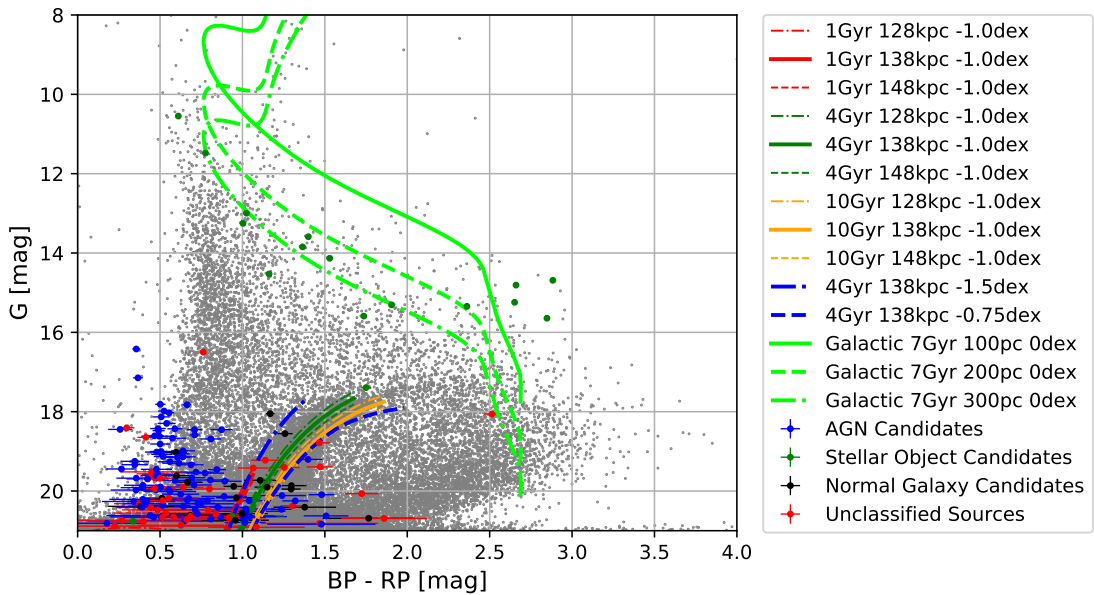


Figure 13: Gaia color-magnitude diagram with isochrones modelling the galactic foreground population and the RGB of the Fornax dSph. The plot also includes all the Gaia sources in the region of the galaxy marked as grey dots.

In the 2MASS color-magnitude diagram, one isochrone was plotted showing the main stellar population at 4 Gyr, 139 kpc and -1.0 dex. For the older population of 10 Gyr

again three isochrones were plotted for the three different distances of 128 kpc, 138 kpc and 148 kpc and with a metallicity of -1.0 dex as well as the aforementioned galactic isochrones.

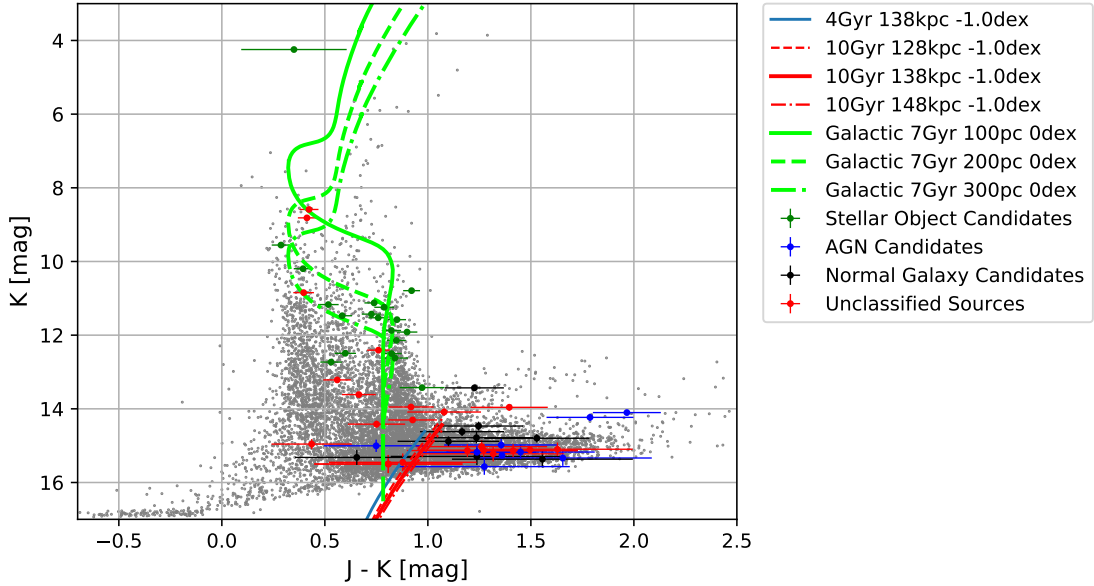


Figure 14: 2MASS color-magnitude diagram of all the matched sources. Similar to the Gaia color-magnitude diagram the isochrones to model the galactic foreground population and the RGB of the Fornax dSph are included. Additionally all the 2MASS sources in the region of the galaxy are again marked as the grey dots.

When taking a more in depth look at the Gaia color-magnitude diagram, an overdensity in the known sources marked as the grey dots can clearly be seen at the location of the isochrones that model the population of Fornax. The isochrones plotted are usually much bigger and extend to higher G-band magnitudes, but the data cannot resolve these extremely faint objects, so what we see in the data set is the end of the Red Giant Branch of the galaxy. The giant branch also aligns quite well with the tested stellar population at 4 Gyr and 10 Gyr, so it is expected that possible stellar X-Ray sources of Fornax should lie on this giant branch or at least very close to it. As can be seen in the plot, the source group, which correlates the most with the giant branch, is the one of the Normal Galaxy Candidates, as also mentioned before. In the region of the Red Giant Branch also some unclassified sources, as well as one Stellar Object Candidate are visible. All these sources have a possibility of being located in the Fornax dSph and need to be analysed further. Regarding the Stellar Object Candidates, most of them align well with the plotted galactic isochrones, so it is quite safe to assume that they are in fact located in the Milky Way and are thus foreground objects. Nevertheless, the Gaia parallax data for all the Stellar Object Candidates was checked. In Table 5, all the Stellar Object Candidates

are shown with their measured parallax distance (rgeo) according to Bailer-Jones et al. (2021). All of the parallax distances correspond with sources in the Milky Way. There is also one unclassified source with source ID 1846 located at the lower end of the galactic isochrones in Figure 13, so it could also be a foreground star. This was also checked manually and indeed the source is a foreground star at a parallax distance of about 300.55 pc (Bailer-Jones et al., 2021).

Regarding the 2MASS data, the Red Giant Branch is also visible in the known 2MASS sources, though not as visible as in the Gaia data. Like in the Gaia data, the isochrones of the Fornax population align well with the Red Giant Branch. In the case of 2MASS also some Normal Galaxy Candidates are in close vicinity of the giant branch, as well as a couple of unclassified sources. Moreover the 2MASS data interestingly shows a few extra unclassified sources in the region of the Galactic isochrones, which will later be analysed further.

Source ID	Ra	Dec	Error	Parallax distance [pc]
930	38.926079	-34.627293	3.495249	806.22509800
1023	39.099049	-34.401516	3.144019	53.91367720
1072	39.179363	-35.080257	4.423796	241.51693700
1111	39.244122	-34.579605	3.00189	25.43659400
1169	39.364029	-34.504429	2.482287	248.24565100
1217	39.462097	-35.58313	2.735987	72.58837130
1231	39.472805	-35.35899	4.327928	321.74279800
1355	39.701229	-34.614395	3.603014	761.92022700
1383	39.748997	-33.483932	4.068282	216.57621800
1448	39.887726	-35.720371	1.47775	91.19542690
1452	39.892448	-34.364326	2.050658	682.42315700
1562	40.080849	-34.547729	3.49973	461.60397300
1581	40.12569	-34.948292	3.463161	258.46972700
1590	40.141129	-34.451519	2.193257	106.63474300
1613	40.178692	-33.712429	3.1891	458.81140100
1634	40.221558	-33.701344	2.066375	313.11978100
1702	40.338341	-33.653721	2.980451	244.94583100
1794	40.510345	-34.927837	2.092262	104.26322900
1895	40.664402	-35.272659	3.93002	158.03308100
2024	40.928696	-34.136623	2.58277	400.57363900

Table 5: The Gaia parallax distances (Bailer-Jones et al., 2021) of the Stellar Object Candidates alongside their coordinates.

2.3.3 Further Classification and Source Properties

With the aim of further classifying the sources, some new plots are discussed in this section. The goal is to check for possible counterparts in Fornax for the Normal Galaxy Candidates and to classify the still unclassified sources. The intention is a narrowed

down selection of unclassified and interesting sources for further research. In this section the Hardness Ratios of the sources, the countrate of eROSITA and a comparison of the W1-band of WISE and the G-band of Gaia will be discussed.

The Hardness Ratios of the sources were calculated according to Saeedi, Sara et al. (2016) with Equation 5 for the Hardness Ratios Equation 6 for their errors.

$$HR_i = \frac{B_{i+1} - B_i}{B_{i+1} + B_i} \quad (5)$$

$$EHR_i = 2 \cdot \sqrt{\frac{(B_{i+1} \cdot EB_i)^2 + (B_i \cdot EB_{i+1})^2}{(B_{i+1} + B_i)^2}} \quad (6)$$

With B_{i+1} and B_i the counts of the higher and lower energy bands respectively and their corresponding errors EB_{i+1} and EB_i . The Hardness Ratios of the sources are shown in Figure 15 and Figure 16. In order to plot the Hardness Ratios, sources which had Hardness Ratio values of 1 or -1 in either Hardness Ratio 1, Hardness Ratio 2 or Hardness Ratio 3 were excluded from the plot. To make the source distribution more visible, the sources are plotted without errorbars. The mean errors of the Hardness Ratios were very high, for Hardness Ratio 1 the mean error was 0.88, for Hardness Ratio 2 0.85 and for Hardness Ratio 3 0.51. The high errors are likely due to the low counts of most of the sources.

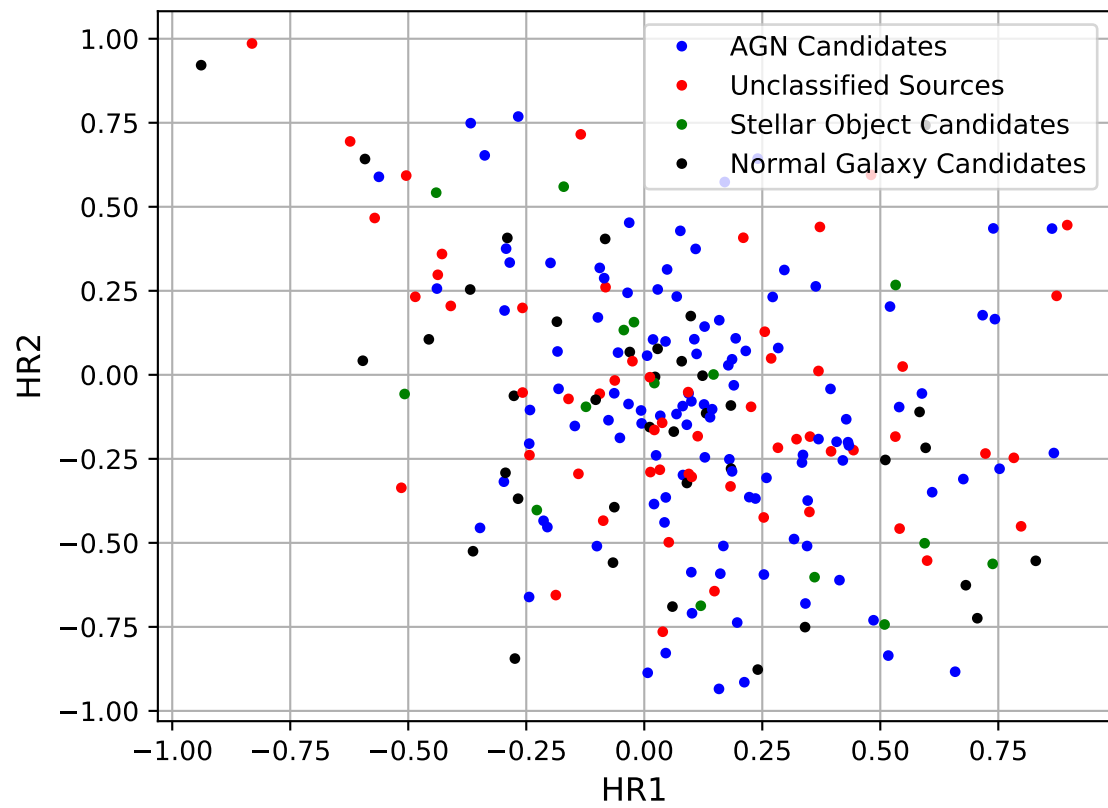


Figure 15: Hardness Ratio 1 plotted against Hardness Ratio 2

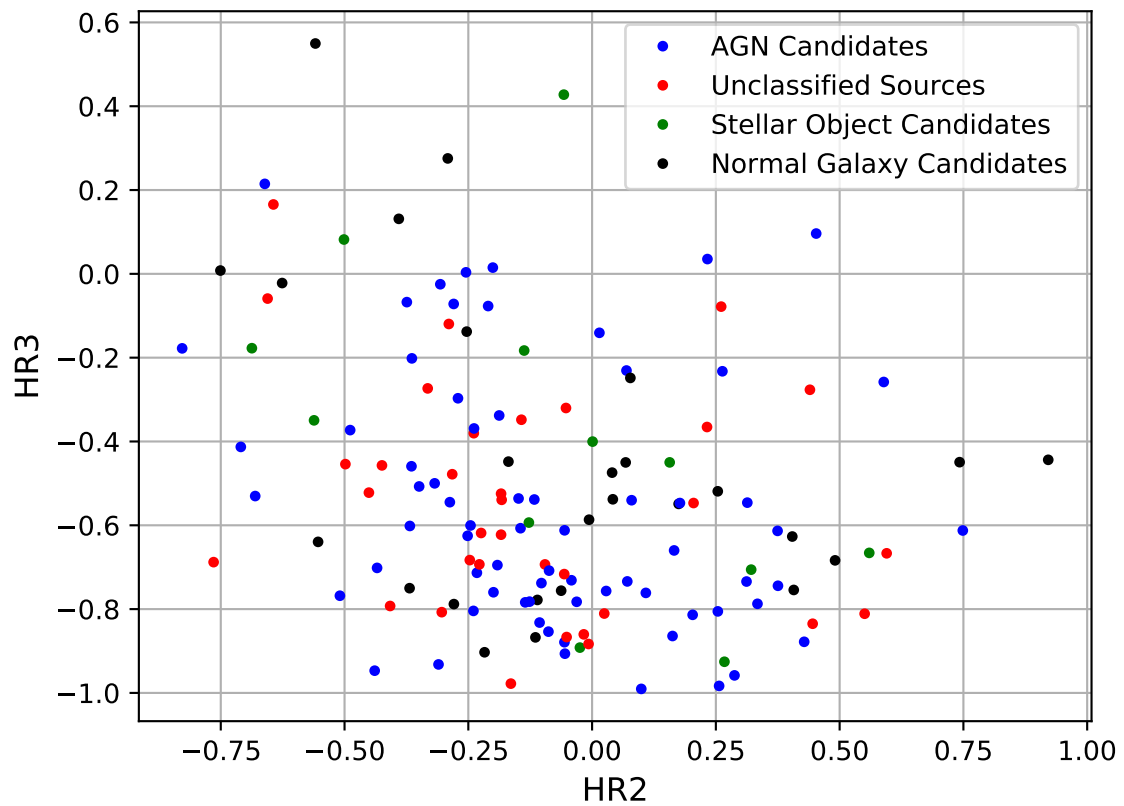


Figure 16: Hardness Ratio 2 plotted against Hardness Ratio 3

Besides the Hardness Ratios, the W1-band of WISE got plotted against the G-band of Gaia. This plot is shown in Figure 17. In this plot again a clear separation between the Stellar Object Candidates and the Normal Galaxy Candidates/AGN Candidates can be observed.

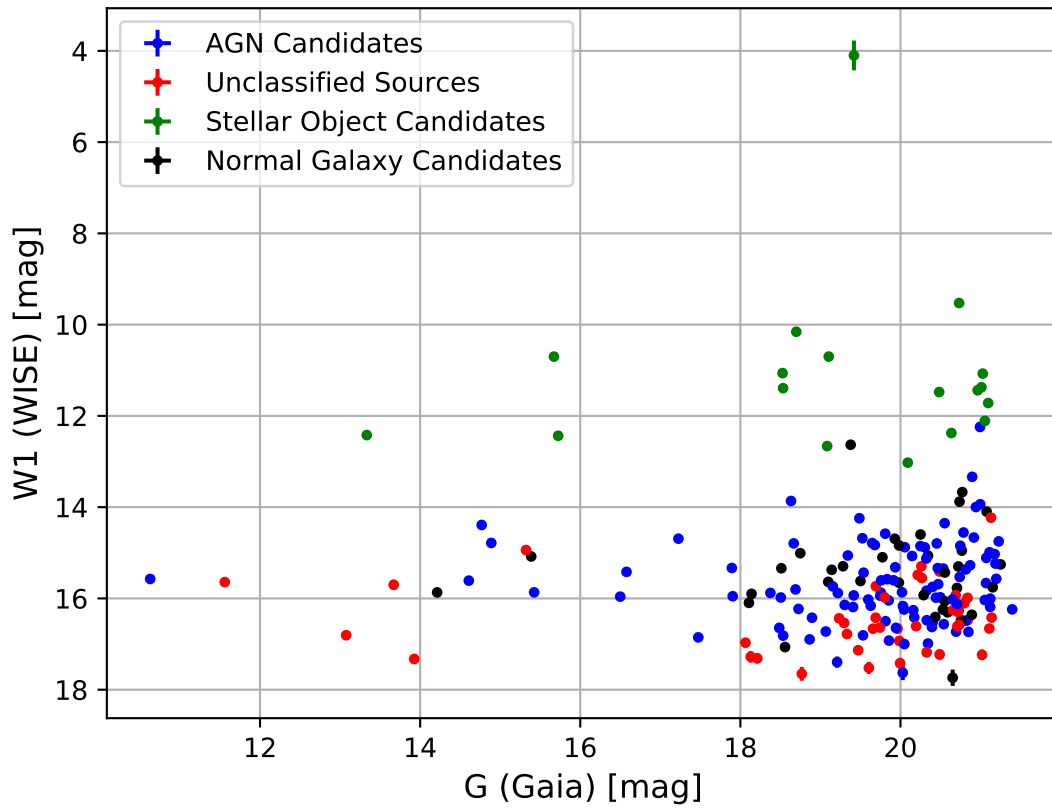


Figure 17: W1 band of the WISE data over the G band of Gaia. The objects are again marked according to the Wright et al. (2010) classification. A clear separation between the Stellar Object Candidates and the Normal Galaxy Candidates/AGN Candidates can be seen.

Figure 18 again shows the G-band magnitude of Gaia, but this time plotted against the source countrate of eROSITA over the entire used energy range.

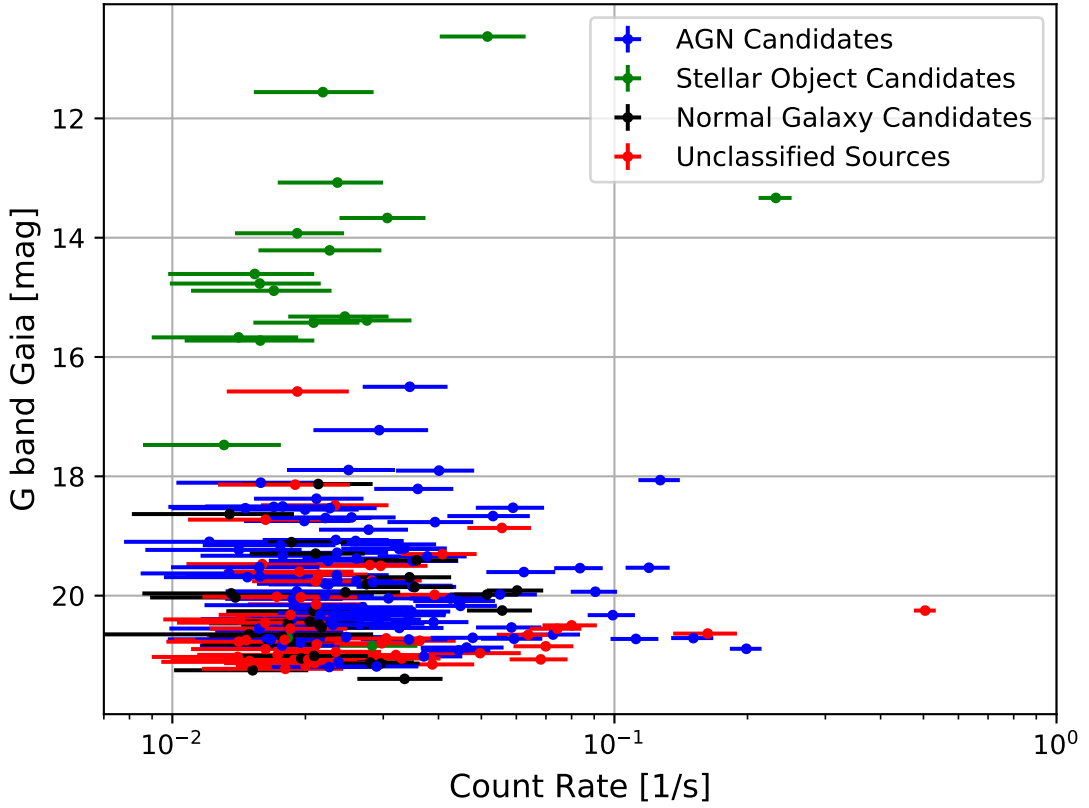


Figure 18: Gaia G band over the X-Ray count rate of eROSITA. The sources are colored according to the Wright et al. (2010) classification.

To investigate possible source candidates for Fornax, all the Normal Galaxy Candidates and unclassified sources residing in the region of the Red Giant Branch, meaning the source error overlaps with the assumed stellar population isochrone of 4 Gyr, 138 kpc and -1.0 dex or the isochrone of 10 Gyr, 138 kpc and -1.0 dex, were checked for potential other catalog matches. The results of the matches are listed in Table 6. For every source a match could be found, though sometimes the search radius had to be increased to two times the source error. The sources which needed an increased search region are also marked in the table. In general the match types were expected to be stars located in the Fornax dSph or background galaxies. This assumption could be confirmed and seven stars located in the galaxy could thus be detected by eROSITA. The rest of the sources were confirmed as background AGNs or galaxies. Some of the sources, namely those which needed an increased search radius, could benefit from further analysis and more data. An extended investigation could for example include a spectral analysis of these sources.

After the rest of the sources, meaning all the confirmed Stellar Objects in the foreground as well as all other AGN and Normal Galaxy Candidates were excluded, there are still some unclassified sources left, which will be discussed in the next section.

ID	Ra	Dec	Error	Catalog Matches	Type
953	38.96265	-34.586792	3.46994	Bate et al. (2015)	Galaxy (2-sigma)
1153	39.319702	-35.568485	4.695148	Bate et al. (2015)	Galaxy (2-sigma)
1177	39.379898	-34.71019	5.371326	Battaglia et al. (2006)	Star*
1218	39.462135	-34.939709	4.386434	Bate et al. (2015)	Galaxy
1224	39.468166	-34.528629	5.72648	de Boer et al. (2012)	Star* (2-sigma)
1236	39.480953	-34.980556	4.059443	de Boer et al. (2012)	Star* (2-sigma)
1413	39.813824	-34.591362	4.045979	Battaglia et al. (2006)	Star*
1422	39.839569	-33.497223	6.202854	Bate et al. (2015)	Galaxy
1433	39.85817	-35.263794	4.165048	Flesch (2021)	AGN (2-sigma)
1486	39.954552	-34.332886	2.913513	Flesch (2021)	AGN
1488	39.956688	-34.240776	3.738324	de Boer et al. (2012)	Star*
1569	40.094688	-33.669006	1.193058	Bate et al. (2015)	Galaxy (2-sigma)
1605	40.162132	-34.649769	1.336226	Flesch (2021)	AGN
1676	40.3013	-34.155972	4.85379	de Boer et al. (2012)	Star*
1758	40.444988	-34.874111	4.156886	Wright et al. (2010)	AGN (2-sigma)
1763	40.451866	-34.996799	3.820982	de Boer et al. (2012)	Star*
1808	40.531715	-33.722294	1.098599	Bate et al. (2015)	Galaxy (2-sigma)
1810	40.53183	-34.665524	0.804559	Helmi et al. (2018)	(2-sigma)
1957	40.815041	-33.935417	2.205818	Bate et al. (2015)	Galaxy
2005	40.899559	-33.842224	4.361297	Flesch (2021)	AGN
2075	41.005634	-34.189018	4.1664	Bate et al. (2015)	Galaxy
2083	41.022984	-33.877151	2.914427	Bate et al. (2015)	Galaxy (2-sigma)

Table 6: Table of all unclassified sources and Normal Galaxy Candidates near the Fornax population isochrones. A 2-sigma behind the Type means, that the search radius had to be increased to two times the Error. All the stars marked with * are already cataloged Fornax sources.

2.3.4 Unclassified Sources

After all the source matching and classification, there are still some unclassified sources missing, namely those, which did not get a counterpart via the matching script in any of the catalogs as well as the unclassified sources of WISE and the ones only identified by Gaia or only by 2MASS not located on the RGB of Fornax. These sources will be examined more closely in this chapter. First of all these sources will be plotted in a counts over Hardness Ratio plot, to first get an idea of how many sources are left, how bright they are and to also see if they are hard or soft sources. This plot can be seen in Figure 19.

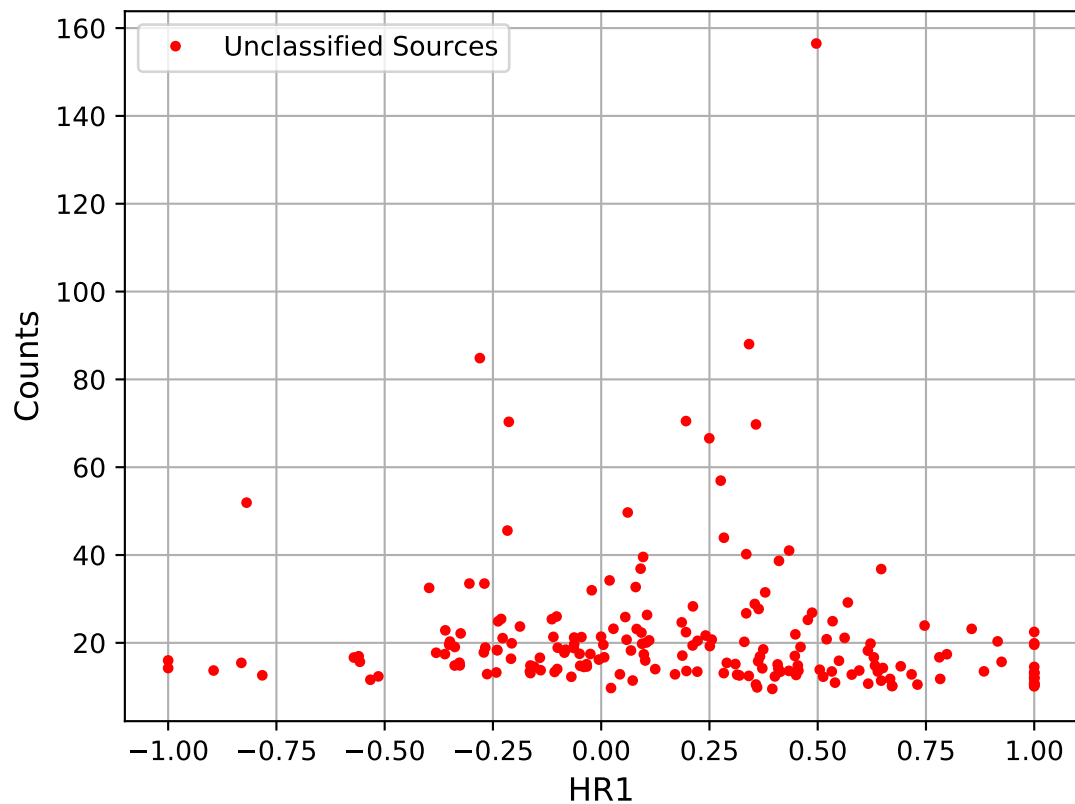


Figure 19: All the still unclassified sources, plotted with their counts over their measured hardness ratio. Most of the sources are quite dim at only around 20 counts.

As can be seen in the Figure 19, there are still some sources left. Though most of them are very faint. Therefore, in order to combat the uncertainties coming with these low counts, only the sources over 50 counts are looked at more closely in the following. Consequently, the respective smaller amount of sources can be examined manually and additionally their source IDs will be shown in the reduced plot in Figure 20.

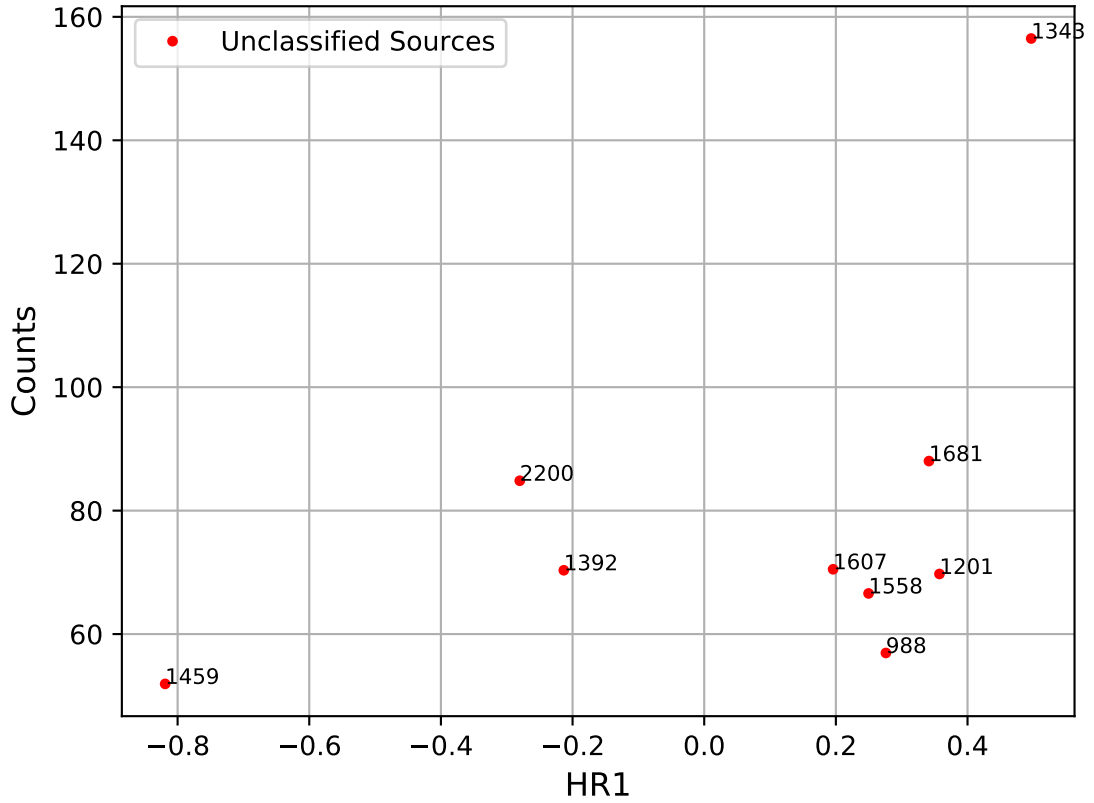


Figure 20: All the sources without catalog matches, but only those which had counts > 50 . Their corresponding sources IDs to the filtered eROSITA catalog are also shown in the plot.

As a result only 9 unclassified sources must be dealt with. This can quite easily be done by searching through online catalogs on VizieR ⁴ manually.

After going through the online catalogs manually a match could be found for all of the sources, except for source 1392. This source has a large error of around 12 arcsec and inside of the error there are multiple possible candidates so it cannot clearly be decided on a counterpart. This source would also benefit from further analysis. Again, like for the sources located near the isochrones, sometimes the search radius had to be increased. The sources, which needed an increased search radius are marked as such in the table. The results of the manual matching as well as the coordinates, the catalogs and the source type can be found in Table 7. As the bright unclassified sources in the regions of the Galactic isochrones in the 2MASS data did not get classified yet, it is not surprising that three additional foreground stars could be found.

⁴ <https://vizier.cds.unistra.fr/viz-bin/VizieR>

ID	Ra	Dec	Error	Catalog Matches	Type
988	39.032902	-33.985298	2.385369	de Boer et al. (2012)	Star* (2-sigma)
1201	39.421738	-34.921764	1.63685	de Boer et al. (2012)	Star* (2-sigma)
1343	39.679436	-34.282555	4.252238	Bailer-Jones et al. (2021)	Star (689.6 pc)
1392	39.776161	-34.307354	11.919825		
1459	39.907993	-33.581226	2.228992	Bailer-Jones et al. (2021)	Star (262.4 pc)
1558	40.078896	-35.391529	9.920523	Bate et al. (2015)	Galaxy
1607	40.163612	-34.80032	1.900442	de Boer et al. (2012)	Star* (2-sigma)
1681	40.309658	-35.419922	1.693669	Bailer-Jones et al. (2021)	Star (163.2 pc)
2200	41.199211	-34.017227	1.668538	Flesch (2021)	AGN (3-sigma)

Table 7: Catalog matches and classifications of the still unclassified sources. If there is a 2- or 3-sigma behind the Type, the search radius had to be increased to 2 or 3 times the Error respectively. The stars marked with * are located in Fornax according to de Boer et al. (2012).

2.4 Comparison to XMM-Study

This section focuses on the results found in the previous section of the eROSITA data and comparing them to a XMM-Newton observation re-analysed by Nucita, A. A. et al. (2013). Apart from the instrument used for the observation, there are a few key differences between the data sets. Firstly, the field of view of the XMM observation is quite small and the observations with eROSITA, as mentioned before, stem from an All Sky Survey. The field of view of the XMM observation was around 30 arcmin, so it is just a bit smaller than the tidal diameter of the galaxy at around 32 arcmin. The field of view worked with, using the eROSITA data is five times the tidal diameter at 170 arcmin for the major axis and 130 arcmin for the minor axis, so also roughly five times larger than the XMM observation in diameter. Because the XMM observation was a dedicated observation of the galaxy, the exposure time was much higher than with the eROSITA data, at around 10 ks compared to roughly 1 ks with eROSITA. So when comparing the observations, the XMM data should be deeper than the eROSITA data inside the galaxy. However with the eROSITA data we additionally get coverage of the outer regions of the galaxy, including also three globular clusters, which could not be observed with XMM. The data extraction regions for XMM and eROSITA, as well as the five globular clusters are shown in Figure 21.

Nucita, A. A. et al. (2013) found 107 X-Ray sources in the galaxy. These sources along the sources detected with eROSITA are shown in Figure 22. Because of the big difference in exposure time, only the brightest sources also show up in the eROSITA data. Cross matching the data, we get 16 common sources, so the XMM-Newton data yields 91 more sources than the eROSITA data. Among the common sources, there are two interesting candidates. Firstly, for source 82 of the XMM data, corresponding to source 1452 of the eROSITA data, Nucita, A. A. et al. (2013) found an entry in the position and proper motions extended catalog (PPMX) (Röser, S. et al., 2008), implying that it is a foreground source. In fact, source 1452 was identified as a Stellar Object Candidate in

the WISE classification and also had a realistic parallax from Bailer-Jones et al. (2021). Secondly, source 107 of the XMM data, corresponding to source 1560 of the eROSITA data, could be identified as a background AGN, which was used as a reference object for measuring the proper motion of sources in the Fornax dSph. Nucita, A. A. et al. (2013) thus report, that source 107 may have been erroneously reported in the PPMX catalog. Furthermore, with the XMM data, Nucita, A. A. et al. (2013) were able to find a variable star, located in the Fornax galaxy with source ID 61, but this source could not be verified with the eROSITA data.

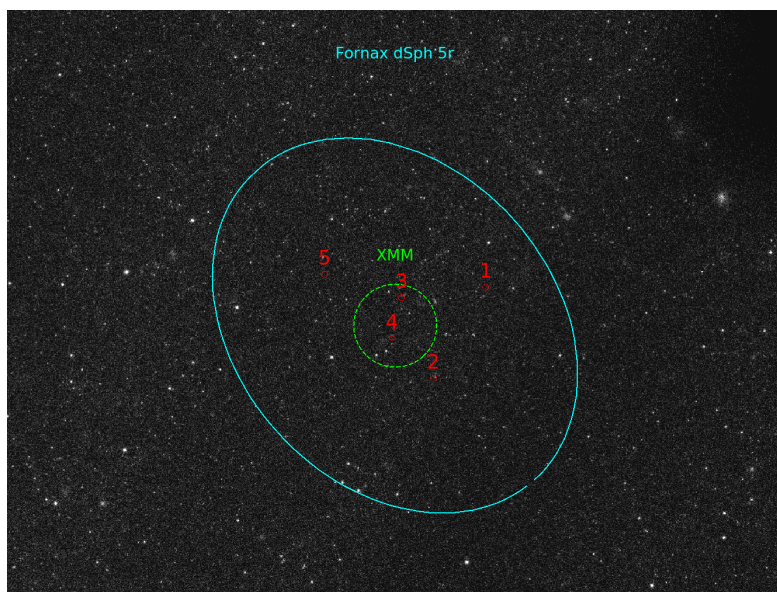
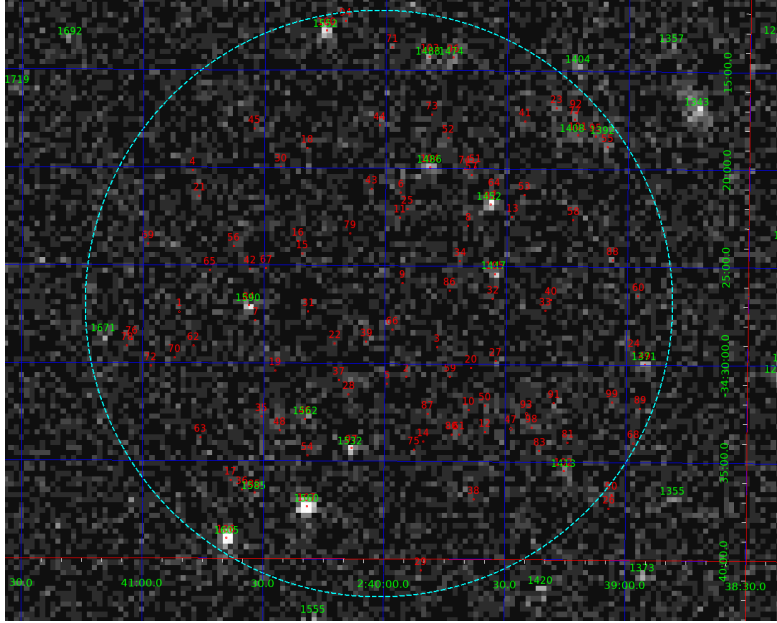


Figure 21: Comparison of the extraction areas from XMM-Newton (Nucita, A. A. et al., 2013) and the eROSITA data. The five globular clusters of Fornax are also marked in red in the picture. It can clearly be seen, that the XMM data only includes globular clusters 3 and 4.



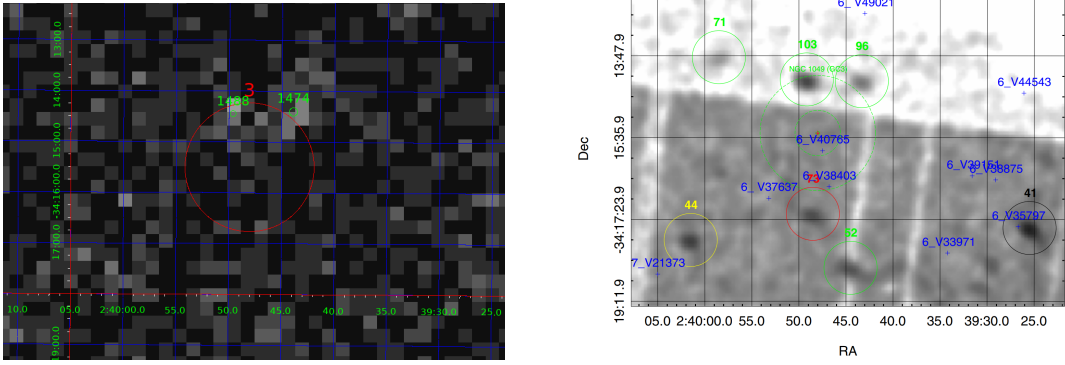


Figure 23: A comparison view of the XMM-Newton data and the eROSITA data for globular cluster 3. Sources 1488 and 1474 correspond to sources 103 and 96 of the XMM data respectively. The other sources around the cluster could not be picked up by eROSITA because of the lower exposure time.

The situation at globular cluster 4, shown in Figure 24 was different. XMM-Newton detected a source, with source ID 28, inside the globular clusters tidal radius, which could not be detected with eROSITA, due to the lower exposure time.

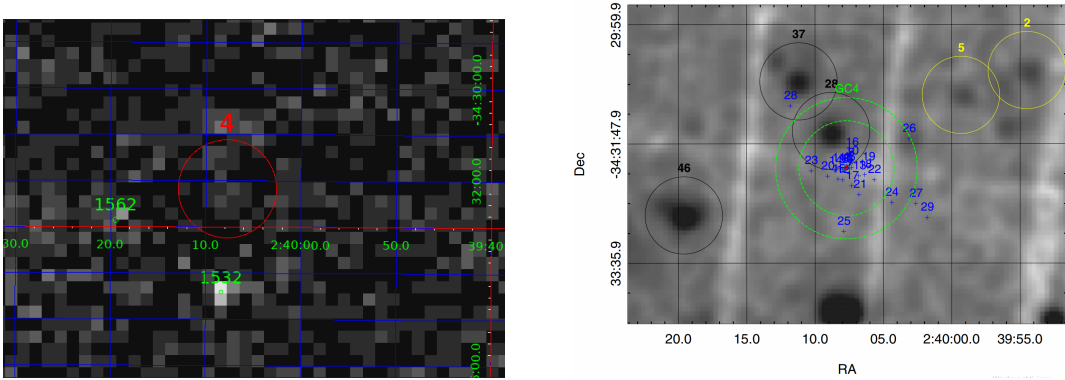


Figure 24: A comparison view of the XMM-Newton data and the eROSITA data for globular cluster 4. The sources 28 and 37 detected with XMM-Newton, which lie closest to the cluster could not be observed with the eROSITA data, probably also because of the lower exposure time.

Regarding the other three globular clusters, which can be only seen in the eROSITA data, clusters 1 and 5 did not show any sources inside their tidal radii. Though globular cluster 2, seen in Figure 25, did show a source inside its tidal radius with source ID 1341. For this source, there is a Gaia DR2 (Gaia Collaboration, 2018) galaxy classification probability of around 58% at a distance of 0.89 arcsec, but also a Fornax star cataloged by de Boer et al. (2012) at a distance of 3.2 arcsec, which lies outside one sigma of the error, but may be worth further investigation. Source 1338 is also cataloged by de Boer

et al. (2012) and is thus a RGB star of the Fornax dSph.

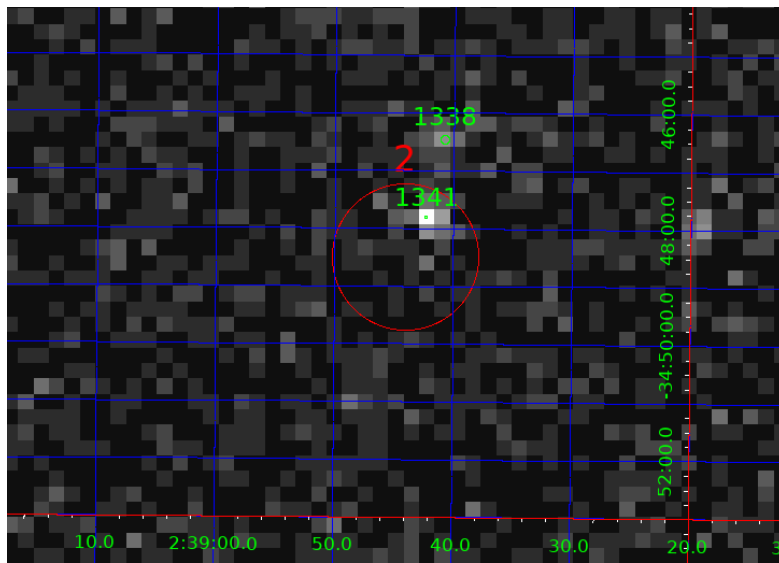


Figure 25: zoomed in eROSITA image of globular cluster 2 showing two sources, one inside the clusters tidal radius and one outside of it.

3 Conclusion

In this thesis, the extracted eROSITA X-Ray sources of three image tiles around the Fornax dSph galaxy were discussed. At first, the sources of the three image tiles were matched with two AGN catalogs, the Milliquas catalog (Flesch, 2021) and the Gaia-WISE Extragalactic Astrometric Catalog (Paine et al., 2018), which yielded 625 matches. On those 625 matches an astrometric correction to the eROSITA data has been performed. After the correction, the source catalog was sorted and filtered on a region with five times the radius of the tidal radius of the galaxy. At this point, the catalog contained 411 sources. This catalog was then used to match the sources to the WISE catalog (Wright et al., 2010), the Gaia DR2 catalog (Gaia Collaboration, 2018) and the 2MASS catalog (Skrutskie et al., 2006). After a first base classification according to ? the sources were plotted in color-magnitude diagrams with the Gaia and 2MASS data. Further source classification could be achieved via matching the sources to isochrones in the diagrams and comparing the different catalog data. All the Normal Galaxy Candidates and unclassified sources, correlating with the population isochrones of Fornax, were inspected for other catalog matches. With these new matches a couple of stars in the Fornax galaxy could be identified. After excluding all the classified foreground and background sources, the still unclassified sources were investigated further. They were filtered to sources with more than 50 counts and then also matched to other catalogs, resulting in three new matches for foreground stars and also three matches for RGB stars in the Fornax dSph. In the last part of the thesis the data set was compared to another XMM-Study executed by Nucita, A. A. et al. (2013). There, another AGN could be identified. This AGN was according to Nucita, A. A. et al. (2013) used as a reference object for measuring the proper motion of sources in the Fornax dSph and may have been erroneously reported in the PPMX catalog. Comparing sources at the globular clusters, a Fornax RGB star which was detected by XMM at globular cluster 3, was also detected by eROSITA. At globular cluster 4 XMM detected a source inside the tidal radius of the cluster. This source could not be resolved with the eROSITA data. At globular cluster 2, which was outside the field of view of XMM, two sources were detected with eROSITA. The source inside the tidal radius could either be a background galaxy or a RGB star of Fornax and would need further research. The source outside the cluster was classified as an RGB star of Fornax.

In total, this work could identify 24 stellar foreground objects, 38 normal galaxies, 131 AGNs and 11 RGB stars inside the Fornax dSph.

Further analysis of this data set could for example be a spectral analysis of the brightest Fornax sources and further investigation of all sources, which needed an increased search region to find a match. Moreover, all the unclassified sources, which were quite dim at less than 50 counts can be analysed further. Also, with the separated eRASS observations, variability of sources on these timescales could be observed which could be interesting, because Nucita, A. A. et al. (2013) did find a variable star which is likely located in the Fornax dSph.

References

- C. A. L. Bailer-Jones, J. Rybizki, M. Fouesneau, M. Demleitner, and R. Andrae. Estimating distances from parallaxes. v. geometric and photogeometric distances to 1.47 billion stars in gaia early data release 3. *The Astronomical Journal*, 161(3): 147, feb 2021. doi: 10.3847/1538-3881/abd806. URL <https://doi.org/10.3847/2F1538-3881%2Fabd806>.
- N. F. Bate, B. McMonigal, G. F. Lewis, M. J. Irwin, E. Gonzalez-Solares, T. Shanks, and N. Metcalfe. The shell game: a panoramic view of Fornax. *Monthly Notices of the Royal Astronomical Society*, 453(1):690–703, 08 2015. ISSN 0035-8711. doi: 10.1093/mnras/stv1684. URL <https://doi.org/10.1093/mnras/stv1684>.
- G. Battaglia, E. Tolstoy, A. Helmi, M. J. Irwin, B. Letarte, P. Jablonka, V. Hill, K. A. Venn, M. D. Shetrone, N. Arimoto, F. Primas, A. Kaufer, P. Francois, T. Szeifert, T. Abel, and K. Sadakane. VizieR Online Data Catalog: VI and [Fe/H] of Fornax dSph RGB stars (Battaglia+, 2006). *VizieR Online Data Catalog*, art. J/A+A/459/423, Nov. 2006.
- D. R. Cole, W. Dehnen, J. I. Read, and M. I. Wilkinson. The mass distribution of the fornax dSph: constraints from its globular cluster distribution. *Monthly Notices of the Royal Astronomical Society*, 426(1):601–613, sep 2012. doi: 10.1111/j.1365-2966.2012.21885.x. URL <https://doi.org/10.1111%2Fj.1365-2966.2012.21885.x>.
- T. J. L. de Boer, E. Tolstoy, V. Hill, A. Saha, E. W. Olszewski, M. Mateo, E. Starkenburg, G. Battaglia, and M. G. Walker. The star formation and chemical evolution history of the fornax dwarf spheroidal galaxy. *Astronomy & Astrophysics*, 544:A73, jul 2012. doi: 10.1051/0004-6361/201219547. URL <https://doi.org/10.1051%2F0004-6361%2F201219547>.
- ESA. Dwarf Galaxies around the Milky Way, 2021a. https://www.esa.int/ESA_Multimedia/Images/2021/11/Dwarf_galaxies_around_the_Milky_Way [Accessed on 2023-01-10].
- ESA. Gaia reveals that most Milky Way companion galaxies are newcomers to our corner of space, 2021b. https://www.esa.int/Science_Exploration/Space_Science/Gaia/Gaia_reveals_that_most_Milky_Way_companion_galaxies_are_newcomers_to_our_corner_of_space [Accessed on 2023-01-10].
- ESA/Hubble. Fornax Picture Hubble, a. <https://esahubble.org/images/heic1425g/> [Accessed on 2023-01-08].
- ESA/Hubble. Fornax Globular Clusters, b. <https://esahubble.org/images/heic1425b/> [Accessed on 2023-01-08].
- ESA/Hubble. Dwarf Galaxy, c. <https://esahubble.org/wordbank/dwarf-galaxy/> [Accessed on 2023-01-10].

- E. W. Flesch. The million quasars (milliquas) v7.2 catalogue, now with vlass associations. the inclusion of sdss-dr16q quasars is detailed, 2021. URL <https://arxiv.org/abs/2105.12985>.
- Gaia Collaboration. Gaia data release 2 - summary of the contents and survey properties. *A&A*, 616:A1, 2018. doi: 10.1051/0004-6361/201833051. URL <https://doi.org/10.1051/0004-6361/201833051>.
- F. Hammer, J. Wang, M. S. Pawlowski, Y. Yang, P. Bonifacio, H. Li, C. Babusiaux, and F. Arenou. Gaiaedr3 proper motions of milky way dwarfs. ii velocities, total energy, and angular momentum. *The Astrophysical Journal*, 922(2):93, nov 2021. doi: 10.3847/1538-4357/ac27a8. URL <https://dx.doi.org/10.3847/1538-4357/ac27a8>.
- A. Helmi, F. van Leeuwen, P. J. McMillan, D. Massari, T. Antoja, A. C. Robin, Lindegren, and G. Collaboration. Gaia Data Release 2. Kinematics of globular clusters and dwarf galaxies around the Milky Way. , 616:A12, Aug. 2018. doi: 10.1051/0004-6361/201832698.
- T. C. Licquia and J. A. Newman. IMPROVED ESTIMATES OF THE MILKY WAY’S STELLAR MASS AND STAR FORMATION RATE FROM HIERARCHICAL BAYESIAN META-ANALYSIS. *The Astrophysical Journal*, 806(1):96, jun 2015. doi: 10.1088/0004-637x/806/1/96. URL <https://doi.org/10.1088/0004-637x/806/1/96>.
- P. Marigo, L. Girardi, A. Bressan, M. A. T. Groenewegen, L. Silva, and G. L. Granato. Evolution of asymptotic giant branch stars. II. Optical to far-infrared isochrones with improved TP-AGB models. , 482(3):883–905, May 2008. doi: 10.1051/0004-6361:20078467.
- M. L. Mateo. Dwarf Galaxies of the Local Group. , 36:435–506, Jan. 1998. doi: 10.1146/annurev.astro.36.1.435.
- Nucita, A. A., Manni, L., De Paolis, F., Vetrugno, D., and Ingrassio, G. An xmm-newton search for x-ray sources in the fornax dwarf galaxy. *A&A*, 550:A18, 2013. doi: 10.1051/0004-6361/201220152. URL <https://doi.org/10.1051/0004-6361/201220152>.
- J. Paine, J. Darling, and A. Truebenbach. Theigaia/i-iWISE/iextragalactic astrometric catalog. *The Astrophysical Journal Supplement Series*, 236(2):37, jun 2018. doi: 10.3847/1538-4365/aabe2d. URL <https://doi.org/10.3847/1538-4365/aabe2d>.
- Predehl, P., Andritschke, R., Arefiev, V., Babyshkin, V., Batanov, O., Becker, W., Böhringer, H., Bogomolov, A., Boller, T., Borm, K., Bornemann, W., Bräuninger, H., Brüggem, M., Brunner, H., Brusa, M., Bulbul, E., Buntov, M., Burwitz, V., Burkert, W., Clerc, N., Churazov, E., Coutinho, D., Dauser, T., Dennerl, K., Doroshenko, V., Eder, J., Emberger, V., Eraerds, T., Finoguenov, A., Freyberg, M., Friedrich, P., Friedrich, S., Fürmetz, M., Georgakakis, A., Gilfanov, M., Granato, S., Grossberger, C., Gueguen, A., Gureev, P., Haberl, F., Hälker, O., Hartner, G., Hasinger, G., Huber,

- H., Ji, L., Kienlin, A. v., Kink, W., Korotkov, F., Kreykenbohm, I., Lamer, G., Lomakin, I., Lapshov, I., Liu, T., Maitra, C., Meidinger, N., Menz, B., Merloni, A., Mernik, T., Mican, B., Mohr, J., Müller, S., Nandra, K., Nazarov, V., Pacaud, F., Pavlinsky, M., Perinati, E., Pfeffermann, E., Pietschner, D., Ramos-Ceja, M. E., Rau, A., Reiffers, J., Reiprich, T. H., Robrade, J., Salvato, M., Sanders, J., Santangelo, A., Sasaki, M., Scheuerle, H., Schmid, C., Schmitt, J., Schwöpe, A., Shirshakov, A., Steinmetz, M., Stewart, I., Strüder, L., Sunyaev, R., Tenzer, C., Tiedemann, L., Trümper, J., Voron, V., Weber, P., Wilms, J., and Yaroshenko, V. The eROSITA x-ray telescope on srg. *A&A*, 647:A1, 2021. doi: 10.1051/0004-6361/202039313. URL <https://doi.org/10.1051/0004-6361/202039313>.
- Röser, S., Schilbach, E., Schwan, H., Kharchenko, N. V., Piskunov, A. E., and Scholz, R.-D. Ppm-extended (ppmx) - a catalogue of positions and proper motions*. *A&A*, 488(1):401–408, 2008. doi: 10.1051/0004-6361:200809775. URL <https://doi.org/10.1051/0004-6361:200809775>.
- Saeedi, Sara, Sasaki, Manami, and Ducci, Lorenzo. Xmm-newton study of the draco dwarf spheroidal galaxy. *A&A*, 586:A64, 2016. doi: 10.1051/0004-6361/201526233. URL <https://doi.org/10.1051/0004-6361/201526233>.
- M. Salvato, J. Buchner, T. Budavári, T. Dwelly, A. Merloni, M. Brusa, A. Rau, S. Fotopoulou, and K. Nandra. Finding counterparts for all-sky X-ray surveys with Nway: a Bayesian algorithm for cross-matching multiple catalogues. *Monthly Notices of the Royal Astronomical Society*, 473(4):4937–4955, 10 2017. ISSN 0035-8711. doi: 10.1093/mnras/stx2651. URL <https://doi.org/10.1093/mnras/stx2651>.
- F. Sestito, N. Longeard, N. F. Martin, E. Starkenburg, M. Fouesneau, J. I. González Hernández, A. Arentsen, R. Ibata, D. S. Aguado, R. G. Carlberg, P. Jablonka, J. F. Navarro, E. Tolstoy, and K. A. Venn. Tracing the formation of the Milky Way through ultra metal-poor stars. , 484(2):2166–2180, Apr. 2019. doi: 10.1093/mnras/stz043.
- H. Shapley. Two stellar systems of a new kind. *Nature*, 142, oct 1938. doi: 10.1038/142715b0. URL <https://doi.org/10.1038/142715b0>.
- M. F. Skrutskie, R. M. Cutri, R. Stiening, M. D. Weinberg, S. Schneider, J. M. Carpenter, C. Beichman, R. Capps, T. Chester, J. Elias, J. Huchra, J. Liebert, C. Lonsdale, D. G. Monet, S. Price, P. Seitzer, T. Jarrett, J. D. Kirkpatrick, J. E. Gizis, E. Howard, T. Evans, J. Fowler, L. Fullmer, R. Hurt, R. Light, E. L. Kopan, K. A. Marsh, H. L. McCallon, R. Tam, S. Van Dyk, and S. Wheelock. The Two Micron All Sky Survey (2MASS). , 131(2):1163–1183, Feb. 2006. doi: 10.1086/498708.
- Uni Tuebingen, Eva Laplace, Inga Saathoff, Chris Tenzer. eROSITA schematic, 2018. <https://uni-tuebingen.de/fakultaeten/mathematisch-naturwissenschaftliche-fakultaet/fachbereiche/physik/institute/astronomie-und-astrophysik/astronomie-hea/forschung/prof-santangelo-abteilung-hochenergieastrophysik/beteiligung-an-experimenten/erosita/> [Accessed on 2023-01-10].

Université de Strasbourg/CNRS. VizieR. <https://vizier.cds.unistra.fr/viz-bin/VizieR> [Accessed on 2023-01-08].

E. L. Wright, P. R. M. Eisenhardt, A. K. Mainzer, M. E. Ressler, R. M. Cutri, T. Jarrett, J. D. Kirkpatrick, D. Padgett, R. S. McMillan, M. Skrutskie, S. A. Stanford, M. Cohen, R. G. Walker, J. C. Mather, D. Leisawitz, T. N. Gautier, I. McLean, D. Benford, C. J. Lonsdale, A. Blain, B. Mendez, W. R. Irace, V. Duval, F. Liu, D. Royer, I. Heinrichsen, J. Howard, M. Shannon, M. Kendall, A. L. Walsh, M. Larsen, J. G. Cardon, S. Schick, M. Schwalm, M. Abid, B. Fabinsky, L. Naes, and C.-W. Tsai. The wide-field infrared survey explorer (wise): Mission description and initial on-orbit performance. *The Astronomical Journal*, 140(6):1868, nov 2010. doi: 10.1088/0004-6256/140/6/1868. URL <https://dx.doi.org/10.1088/0004-6256/140/6/1868>.

4 Acknowledgements

Many thanks to my supervisor Prof. Manami Sasaki for this Bachelor thesis topic and also for regularly answering questions and supporting me through the thesis. I would like to extend my thanks to Sara Saeedi, who also constantly supported me through the thesis and helped me with the data analysis. Thank you to Jonathan Knies for the Artemis matching script, used in this thesis and for helping me to get it up and running. Additionally I would like to thank Marie Prucker for providing a Latex template and also for her support during the thesis.

This work is based on the data from the eROSITA telescope on board of the Russian-German Spektr-RG space observatory.

For the data analysis, this thesis used data from the European Space Agency mission Gaia, from the 2MASS mission, which is a joint mission of the University of Massachusetts (UMASS) and the Infrared Processing and Analysis Center (IPAC) at the California Institute of Technology. Furthermore data from the Wide-field Infrared Survey Explorer, which is a joint project of the University of California, Los Angeles, and the Jet Propulsion Laboratory/California Institute of Technology, funded by the National Aeronautics and Space Administration was used.

5 Appendix

ID	Ra	Dec	Error	Catalog Matches	Type
988	39.032902	-33.985298	2.385369	de Boer et al. (2012)	Star (2-sigma)
1177	39.379898	-34.71019	5.371326	Battaglia et al. (2006)	Star
1201	39.421738	-34.921764	1.63685	de Boer et al. (2012)	Star (2-sigma)
1224	39.468166	-34.528629	5.72648	de Boer et al. (2012)	Star (2-sigma)
1236	39.480953	-34.980556	4.059443	de Boer et al. (2012)	Star (2-sigma)
1338	39.66975	-34.77454	4.831741	de Boer et al. (2012)	Star
1413	39.813824	-34.591362	4.045979	Battaglia et al. (2006)	Star
1488	39.956688	-34.240776	3.738324	de Boer et al. (2012)	Star
1607	40.163612	-34.80032	1.900442	de Boer et al. (2012)	Star (2-sigma)
1676	40.3013	-34.155972	4.85379	de Boer et al. (2012)	Star
1763	40.451866	-34.996799	3.820982	de Boer et al. (2012)	Star

Table 8: Table of all the detected sources with counterparts in catalogs of the Fornax dSph.

ID	Ra	Dec	Error
894	3.886306000000E+01	-3.500363200000E+01	6.120635000000E+00
899	3.886813000000E+01	-3.476259200000E+01	3.728463000000E+00
904	3.887653000000E+01	-3.458016600000E+01	6.600642000000E+00
913	3.889154100000E+01	-3.429974700000E+01	3.617327000000E+00
914	3.889428300000E+01	-3.491867100000E+01	4.030570000000E+00
920	3.891195700000E+01	-3.488365900000E+01	5.031511000000E+00
923	3.891722100000E+01	-3.531279400000E+01	3.574025000000E+00
925	3.891986500000E+01	-3.429933200000E+01	4.449053000000E+00
928	3.892419400000E+01	-3.426594200000E+01	4.180884000000E+00
929	3.892586500000E+01	-3.502965900000E+01	2.711937000000E+00
930	3.892607900000E+01	-3.462729300000E+01	3.495249000000E+00
940	3.894167300000E+01	-3.470157600000E+01	4.571111000000E+00
941	3.894244800000E+01	-3.451371400000E+01	2.968160000000E+00
943	3.894712800000E+01	-3.495743900000E+01	4.651539000000E+00
953	3.896265000000E+01	-3.458679200000E+01	3.469940000000E+00
966	3.898372700000E+01	-3.518081300000E+01	3.904539000000E+00
972	3.900067100000E+01	-3.500750400000E+01	4.695560000000E+00
978	3.901429700000E+01	-3.460862400000E+01	4.772573000000E+00
980	3.901980600000E+01	-3.531174100000E+01	3.867248000000E+00
982	3.902016400000E+01	-3.537548100000E+01	3.600867000000E+00
988	3.903290200000E+01	-3.398529800000E+01	2.385369000000E+00
993	3.903960000000E+01	-3.418544800000E+01	1.209308000000E+00
994	3.904146200000E+01	-3.468976600000E+01	4.740771000000E+00

1001	3.906476200000E+01	-3.430312700000E+01	4.411397000000E+00
1005	3.906757700000E+01	-3.417508300000E+01	3.745096000000E+00
1007	3.906964900000E+01	-3.413622700000E+01	4.617686000000E+00
1018	3.908629200000E+01	-3.452489900000E+01	4.028741000000E+00
1020	3.909628300000E+01	-3.513205300000E+01	3.676638000000E+00
1023	3.909904900000E+01	-3.440151600000E+01	3.144019000000E+00
1028	3.910526300000E+01	-3.383160800000E+01	3.163000000000E+00
1029	3.910864300000E+01	-3.468479900000E+01	5.024259000000E+00
1035	3.912414600000E+01	-3.408474000000E+01	2.690376000000E+00
1042	3.913280500000E+01	-3.427932700000E+01	4.315265000000E+00
1049	3.914341700000E+01	-3.543404800000E+01	3.523093000000E+00
1059	3.915594900000E+01	-3.488538400000E+01	5.420176000000E+00
1067	3.916623700000E+01	-3.477203000000E+01	5.874223000000E+00
1070	3.917449200000E+01	-3.400550100000E+01	3.952704000000E+00
1071	3.917675800000E+01	-3.518119800000E+01	8.613266000000E+00
1072	3.917936300000E+01	-3.508025700000E+01	4.423796000000E+00
1073	3.918088900000E+01	-3.534867100000E+01	3.320405000000E+00
1081	3.918683200000E+01	-3.480092600000E+01	4.093281000000E+00
1091	3.921039600000E+01	-3.440688700000E+01	4.442196000000E+00
1100	3.922394600000E+01	-3.469907000000E+01	3.465245000000E+00
1104	3.923443200000E+01	-3.484547000000E+01	1.954165000000E+00
1105	3.923471800000E+01	-3.459677100000E+01	4.151909000000E+00
1109	3.924181400000E+01	-3.371288300000E+01	3.840049000000E+00
1110	3.924406400000E+01	-3.387722800000E+01	1.059700000000E+00
1111	3.924412200000E+01	-3.457960500000E+01	3.001890000000E+00
1112	3.924439600000E+01	-3.474993100000E+01	3.416794000000E+00
1115	3.924533800000E+01	-3.491590900000E+01	4.357410000000E+00
1117	3.925280800000E+01	-3.527354000000E+01	2.944580000000E+00
1119	3.925386000000E+01	-3.519400400000E+01	2.833015000000E+00
1120	3.925518400000E+01	-3.496765900000E+01	4.132144000000E+00
1124	3.926244400000E+01	-3.509153000000E+01	5.084980000000E+00
1125	3.926265700000E+01	-3.365104700000E+01	4.986588000000E+00
1128	3.927015300000E+01	-3.507100700000E+01	3.170946000000E+00
1131	3.927869400000E+01	-3.520980800000E+01	7.044723000000E+00
1132	3.927974300000E+01	-3.424015800000E+01	3.795281000000E+00
1138	3.930124300000E+01	-3.556641400000E+01	4.558825000000E+00
1142	3.930381800000E+01	-3.424950000000E+01	2.644706000000E+00
1143	3.930583600000E+01	-3.519510300000E+01	1.832180000000E+00
1145	3.931089000000E+01	-3.368658100000E+01	2.456384000000E+00
1146	3.931100800000E+01	-3.442044800000E+01	4.003108000000E+00
1148	3.931390000000E+01	-3.416322300000E+01	3.964161000000E+00
1153	3.931970200000E+01	-3.556848500000E+01	4.695148000000E+00
1155	3.932462300000E+01	-3.418096200000E+01	4.031034000000E+00
1158	3.933689900000E+01	-3.371687300000E+01	4.792163000000E+00

1160	3.934269700000E+01	-3.421093400000E+01	2.197703000000E+00
1163	3.935390500000E+01	-3.451110500000E+01	3.024744000000E+00
1164	3.935403100000E+01	-3.368695800000E+01	3.959035000000E+00
1166	3.935755200000E+01	-3.357940300000E+01	1.676275000000E+00
1168	3.936283100000E+01	-3.512742200000E+01	4.389215000000E+00
1169	3.936402900000E+01	-3.450442900000E+01	2.482287000000E+00
1171	3.937168500000E+01	-3.408845500000E+01	3.816170000000E+00
1176	3.937938700000E+01	-3.459722500000E+01	4.148207000000E+00
1177	3.937989800000E+01	-3.471019000000E+01	5.371326000000E+00
1178	3.938332000000E+01	-3.511222500000E+01	3.197586000000E+00
1183	3.939305900000E+01	-3.436389900000E+01	7.660730000000E+00
1189	3.940490700000E+01	-3.526220300000E+01	4.120817000000E+00
1192	3.940839800000E+01	-3.532307400000E+01	4.233927000000E+00
1194	3.941103700000E+01	-3.448149900000E+01	3.464212000000E+00
1195	3.941298300000E+01	-3.482165100000E+01	3.701339000000E+00
1196	3.941529100000E+01	-3.368080500000E+01	3.847881000000E+00
1197	3.941786600000E+01	-3.479442200000E+01	6.963237000000E+00
1201	3.942173800000E+01	-3.492176400000E+01	1.636850000000E+00
1210	3.945080600000E+01	-3.390329400000E+01	2.738296000000E+00
1214	3.945885500000E+01	-3.367167700000E+01	4.262521000000E+00
1216	3.946140700000E+01	-3.383255800000E+01	2.696162000000E+00
1217	3.946209700000E+01	-3.558313000000E+01	2.735987000000E+00
1218	3.946213500000E+01	-3.493970900000E+01	4.386434000000E+00
1219	3.946262400000E+01	-3.423012900000E+01	4.242380000000E+00
1222	3.946462200000E+01	-3.551272600000E+01	5.000716000000E+00
1223	3.946488600000E+01	-3.500669900000E+01	3.735923000000E+00
1224	3.946816600000E+01	-3.452862900000E+01	5.726480000000E+00
1225	3.946859000000E+01	-3.452916700000E+01	3.973668549020E+00
1226	3.946990200000E+01	-3.509951800000E+01	5.420090000000E+00
1227	3.947108800000E+01	-3.424719600000E+01	3.907176000000E+00
1230	3.947220600000E+01	-3.539416100000E+01	5.609039000000E+00
1231	3.947280500000E+01	-3.535899000000E+01	4.327928000000E+00
1232	3.947317100000E+01	-3.363629200000E+01	3.482249000000E+00
1235	3.947831300000E+01	-3.384492900000E+01	4.279410000000E+00
1236	3.948095300000E+01	-3.498055600000E+01	4.059443000000E+00
1238	3.948749900000E+01	-3.492871500000E+01	4.999270000000E+00
1244	3.950258300000E+01	-3.451138300000E+01	3.443315000000E+00
1258	3.953582400000E+01	-3.346820400000E+01	7.232997000000E+00
1262	3.954410900000E+01	-3.341429500000E+01	4.389365000000E+00
1266	3.954934300000E+01	-3.354690600000E+01	4.377704000000E+00
1268	3.955176900000E+01	-3.361554300000E+01	3.797172000000E+00
1270	3.955381000000E+01	-3.451085700000E+01	4.713296000000E+00
1274	3.955623200000E+01	-3.425791900000E+01	3.478447000000E+00
1281	3.957136200000E+01	-3.472540300000E+01	3.904203000000E+00

1283	3.957356300000E+01	-3.505902100000E+01	4.346161000000E+00
1285	3.957477600000E+01	-3.393695400000E+01	2.433458000000E+00
1287	3.957584000000E+01	-3.564304000000E+01	3.601978000000E+00
1288	3.957992900000E+01	-3.479853800000E+01	4.006438000000E+00
1290	3.958477800000E+01	-3.357538200000E+01	3.923547000000E+00
1291	3.958573200000E+01	-3.449987000000E+01	2.095095000000E+00
1292	3.958617800000E+01	-3.439529400000E+01	4.143054000000E+00
1294	3.958846700000E+01	-3.527796600000E+01	5.927054000000E+00
1296	3.959135100000E+01	-3.370912900000E+01	2.740877000000E+00
1297	3.959418900000E+01	-3.450976900000E+01	2.993593000000E+00
1298	3.959782000000E+01	-3.394041800000E+01	2.911341000000E+00
1299	3.959840000000E+01	-3.422095500000E+01	4.277689000000E+00
1305	3.960989400000E+01	-3.376447300000E+01	4.116983000000E+00
1308	3.961759600000E+01	-3.401093300000E+01	2.644924000000E+00
1311	3.962366900000E+01	-3.417286300000E+01	6.115417000000E+00
1313	3.962454200000E+01	-3.504239300000E+01	3.607006000000E+00
1316	3.963053500000E+01	-3.411047700000E+01	3.691443000000E+00
1319	3.963684800000E+01	-3.396006000000E+01	6.623912000000E+00
1320	3.964053000000E+01	-3.354368600000E+01	4.835022000000E+00
1324	3.965346900000E+01	-3.380725500000E+01	5.006397000000E+00
1333	3.966288400000E+01	-3.403815500000E+01	3.804656000000E+00
1334	3.966569100000E+01	-3.491552000000E+01	4.731784000000E+00
1337	3.966962100000E+01	-3.396339000000E+01	3.024381000000E+00
1338	3.966975000000E+01	-3.477454000000E+01	4.831741000000E+00
1340	3.967458000000E+01	-3.548528700000E+01	3.469211000000E+00
1341	3.967602900000E+01	-3.479706200000E+01	1.608307000000E+00
1343	3.967943600000E+01	-3.428255500000E+01	4.252238000000E+00
1345	3.968266300000E+01	-3.473123200000E+01	3.262321000000E+00
1346	3.968478400000E+01	-3.368219800000E+01	6.773144000000E+00
1349	3.969268400000E+01	-3.387797200000E+01	4.364666000000E+00
1350	3.969615200000E+01	-3.412996700000E+01	2.603169000000E+00
1354	3.969743300000E+01	-3.551948900000E+01	1.632547000000E+00
1355	3.970122900000E+01	-3.461439500000E+01	3.603014000000E+00
1357	3.970612700000E+01	-3.422823300000E+01	3.601589000000E+00
1359	3.970978500000E+01	-3.549910700000E+01	4.752742000000E+00
1362	3.971451200000E+01	-3.401113900000E+01	3.524934000000E+00
1363	3.971765500000E+01	-3.568686300000E+01	2.809097000000E+00
1366	3.972376600000E+01	-3.383229100000E+01	2.972426000000E+00
1367	3.972771800000E+01	-3.378810100000E+01	2.049287000000E+00
1368	3.972791700000E+01	-3.498153700000E+01	3.113092000000E+00
1369	3.973069400000E+01	-3.494042200000E+01	2.555331000000E+00
1371	3.973154800000E+01	-3.449987400000E+01	3.534871000000E+00
1373	3.973180800000E+01	-3.468016800000E+01	3.032443000000E+00
1379	3.974099000000E+01	-3.508373300000E+01	4.745258000000E+00

1383	3.974899700000E+01	-3.348393200000E+01	4.068282000000E+00
1385	3.976260400000E+01	-3.399924900000E+01	2.889909000000E+00
1389	3.977096200000E+01	-3.409651600000E+01	5.506666000000E+00
1392	3.977616100000E+01	-3.430735400000E+01	1.191982500000E+01
1393	3.977713400000E+01	-3.357726700000E+01	1.802143000000E+00
1396	3.979145100000E+01	-3.401838700000E+01	4.347733000000E+00
1403	3.980168900000E+01	-3.357397100000E+01	1.614983000000E+00
1404	3.980224600000E+01	-3.424673100000E+01	3.755534000000E+00
1406	3.980530500000E+01	-3.534116700000E+01	6.183157000000E+00
1407	3.980722400000E+01	-3.524029500000E+01	3.289893000000E+00
1408	3.980782300000E+01	-3.430575600000E+01	7.573940000000E+00
1410	3.980899000000E+01	-3.411806900000E+01	4.828526000000E+00
1412	3.981221400000E+01	-3.515705500000E+01	3.779455000000E+00
1413	3.981382400000E+01	-3.459136200000E+01	4.045979000000E+00
1420	3.983700200000E+01	-3.469124200000E+01	2.924521000000E+00
1422	3.983956900000E+01	-3.349722300000E+01	6.202854000000E+00
1424	3.984528000000E+01	-3.340956100000E+01	3.059616000000E+00
1426	3.984622200000E+01	-3.488482300000E+01	3.972407000000E+00
1430	3.985379400000E+01	-3.409279600000E+01	3.694555000000E+00
1433	3.985817000000E+01	-3.526379400000E+01	4.165048000000E+00
1439	3.986567700000E+01	-3.554436900000E+01	4.515283000000E+00
1441	3.986941500000E+01	-3.338252300000E+01	1.772239000000E+00
1443	3.987822700000E+01	-3.483229400000E+01	2.153924000000E+00
1447	3.988745100000E+01	-3.442310700000E+01	2.772281000000E+00
1448	3.988772600000E+01	-3.572037100000E+01	1.477750000000E+00
1449	3.988875600000E+01	-3.550393700000E+01	4.195136000000E+00
1452	3.989244800000E+01	-3.436432600000E+01	2.050658000000E+00
1454	3.989595000000E+01	-3.511755800000E+01	2.624563000000E+00
1457	3.990560200000E+01	-3.350627900000E+01	1.445619800000E+01
1459	3.990799300000E+01	-3.358122600000E+01	2.228992000000E+00
1470	3.992727700000E+01	-3.544545000000E+01	4.736047000000E+00
1472	3.992853200000E+01	-3.564759400000E+01	3.904225000000E+00
1474	3.993277000000E+01	-3.424027600000E+01	5.115356000000E+00
1475	3.993426500000E+01	-3.506170700000E+01	2.685557000000E+00
1481	3.995110300000E+01	-3.488140500000E+01	3.970818000000E+00
1486	3.995455200000E+01	-3.433288600000E+01	2.913513000000E+00
1488	3.995668800000E+01	-3.424077600000E+01	3.738324000000E+00
1496	3.996820800000E+01	-3.553696800000E+01	2.491703000000E+00
1497	3.996826900000E+01	-3.517804000000E+01	4.828419000000E+00
1500	3.997633000000E+01	-3.337299700000E+01	4.430144000000E+00
1502	3.997856500000E+01	-3.390514800000E+01	2.620887000000E+00
1505	3.998233400000E+01	-3.559829300000E+01	3.973668549020E+00
1506	3.998311600000E+01	-3.417540700000E+01	3.180204000000E+00
1510	3.998641600000E+01	-3.333927200000E+01	4.502310000000E+00

1514	3.999474300000E+01	-3.412142600000E+01	3.033132000000E+00
1528	4.003392800000E+01	-3.376166500000E+01	6.426891000000E+00
1529	4.003413000000E+01	-3.397474700000E+01	3.602046000000E+00
1530	4.003431300000E+01	-3.548845300000E+01	4.038094000000E+00
1532	4.003456900000E+01	-3.457359300000E+01	2.355447000000E+00
1533	4.003522100000E+01	-3.362019700000E+01	4.512959000000E+00
1535	4.003659400000E+01	-3.541194900000E+01	5.075745000000E+00
1536	4.004009200000E+01	-3.395747800000E+01	3.834749000000E+00
1537	4.004495600000E+01	-3.389387900000E+01	7.274562000000E+00
1539	4.004711200000E+01	-3.481868000000E+01	3.589482000000E+00
1543	4.005071300000E+01	-3.388439200000E+01	3.971475000000E+00
1549	4.005740000000E+01	-3.365126800000E+01	2.937336000000E+00
1551	4.006263400000E+01	-3.542167300000E+01	1.093461900000E+01
1552	4.006271000000E+01	-3.421773100000E+01	1.894441000000E+00
1554	4.006768400000E+01	-3.544638800000E+01	4.084775000000E+00
1555	4.007215100000E+01	-3.471710600000E+01	3.814705000000E+00
1557	4.007587400000E+01	-3.473045700000E+01	3.070754000000E+00
1558	4.007889600000E+01	-3.539152900000E+01	9.920523000000E+00
1560	4.007961700000E+01	-3.462236000000E+01	1.157980000000E+00
1561	4.008011200000E+01	-3.395726400000E+01	4.002857000000E+00
1562	4.008084900000E+01	-3.454772900000E+01	3.499730000000E+00
1564	4.008470500000E+01	-3.364946700000E+01	4.020693000000E+00
1565	4.008682300000E+01	-3.540243500000E+01	4.208427000000E+00
1568	4.009304000000E+01	-3.387577400000E+01	5.542625000000E+00
1569	4.009468800000E+01	-3.366900600000E+01	1.193058000000E+00
1570	4.009472700000E+01	-3.509771300000E+01	2.531483000000E+00
1571	4.009534500000E+01	-3.552867100000E+01	3.632332000000E+00
1581	4.012569000000E+01	-3.494829200000E+01	3.463161000000E+00
1585	4.013429300000E+01	-3.461171000000E+01	5.742726000000E+00
1588	4.013773300000E+01	-3.358552900000E+01	5.310926000000E+00
1590	4.014112900000E+01	-3.445151900000E+01	2.193257000000E+00
1591	4.014342900000E+01	-3.373261600000E+01	3.140662000000E+00
1595	4.014802600000E+01	-3.414757200000E+01	4.620954000000E+00
1598	4.015079500000E+01	-3.502053500000E+01	2.755590000000E+00
1599	4.015110800000E+01	-3.365844300000E+01	2.694751000000E+00
1601	4.015314900000E+01	-3.562779600000E+01	6.366469000000E+00
1604	4.015968700000E+01	-3.556611300000E+01	4.052250000000E+00
1605	4.016213200000E+01	-3.464976900000E+01	1.336226000000E+00
1607	4.016361200000E+01	-3.480032000000E+01	1.900442000000E+00
1611	4.016848000000E+01	-3.546138400000E+01	1.515915000000E+00
1613	4.017869200000E+01	-3.371242900000E+01	3.189100000000E+00
1615	4.018105300000E+01	-3.551205100000E+01	4.590435000000E+00
1618	4.018951800000E+01	-3.383367500000E+01	4.063493000000E+00
1619	4.018968600000E+01	-3.512107100000E+01	4.467444000000E+00

1621	4.019184500000E+01	-3.487143300000E+01	3.601476000000E+00
1623	4.019895200000E+01	-3.400609200000E+01	3.288315000000E+00
1624	4.020135100000E+01	-3.345640900000E+01	4.376875000000E+00
1631	4.021354700000E+01	-3.365799000000E+01	3.199450000000E+00
1634	4.022155800000E+01	-3.370134400000E+01	2.066375000000E+00
1642	4.023702600000E+01	-3.516919700000E+01	3.409742000000E+00
1648	4.024766500000E+01	-3.554208400000E+01	7.161386000000E+00
1650	4.025120200000E+01	-3.474170700000E+01	4.674329000000E+00
1651	4.025764800000E+01	-3.523203700000E+01	4.774654000000E+00
1654	4.027098800000E+01	-3.328045300000E+01	4.077876000000E+00
1657	4.027328900000E+01	-3.380847200000E+01	4.860799000000E+00
1660	4.027711500000E+01	-3.499234400000E+01	4.448851000000E+00
1665	4.028390100000E+01	-3.352362800000E+01	5.313473000000E+00
1668	4.028696100000E+01	-3.378319900000E+01	2.530770000000E+00
1670	4.028906600000E+01	-3.520340700000E+01	4.027479000000E+00
1671	4.029024500000E+01	-3.447775300000E+01	3.902829000000E+00
1674	4.029978900000E+01	-3.324980500000E+01	2.772990000000E+00
1675	4.030033500000E+01	-3.330418800000E+01	4.999052000000E+00
1676	4.030130000000E+01	-3.415597200000E+01	4.853790000000E+00
1677	4.030238700000E+01	-3.409223200000E+01	2.096663000000E+00
1680	4.030816300000E+01	-3.403551900000E+01	3.397231000000E+00
1681	4.030965800000E+01	-3.541992200000E+01	1.693669000000E+00
1687	4.031985100000E+01	-3.365308800000E+01	2.677294000000E+00
1689	4.032154500000E+01	-3.524128300000E+01	4.072503000000E+00
1692	4.032529800000E+01	-3.422472400000E+01	4.748479000000E+00
1699	4.033350000000E+01	-3.418432200000E+01	4.141946000000E+00
1700	4.033481600000E+01	-3.540837900000E+01	2.794728000000E+00
1701	4.033505200000E+01	-3.405020100000E+01	4.910151000000E+00
1702	4.033834100000E+01	-3.365372100000E+01	2.980451000000E+00
1703	4.033902700000E+01	-3.367224500000E+01	3.525290000000E+00
1705	4.034318200000E+01	-3.372768400000E+01	4.118488000000E+00
1712	4.035584600000E+01	-3.359440600000E+01	4.097910000000E+00
1715	4.036598200000E+01	-3.370519300000E+01	3.377564000000E+00
1717	4.037471400000E+01	-3.343455100000E+01	3.831650000000E+00
1719	4.037962300000E+01	-3.426613200000E+01	5.671569000000E+00
1722	4.038882400000E+01	-3.338175200000E+01	4.698555000000E+00
1723	4.039344400000E+01	-3.539135700000E+01	1.242531000000E+00
1726	4.039492400000E+01	-3.408686100000E+01	4.270007000000E+00
1727	4.039596600000E+01	-3.380029700000E+01	9.055352000000E+00
1732	4.040623100000E+01	-3.362915800000E+01	4.779562000000E+00
1733	4.040645200000E+01	-3.365787100000E+01	1.763771000000E+00
1734	4.040667300000E+01	-3.401322900000E+01	3.919538000000E+00
1735	4.040769600000E+01	-3.430186100000E+01	3.720059000000E+00
1739	4.041021000000E+01	-3.426990100000E+01	2.187526000000E+00

1744	4.041843000000E+01	-3.410189100000E+01	2.300081000000E+00
1745	4.041904100000E+01	-3.356984700000E+01	2.492177000000E+00
1750	4.042427800000E+01	-3.396797600000E+01	3.208873000000E+00
1754	4.044356900000E+01	-3.375972400000E+01	1.706726000000E+00
1756	4.044443100000E+01	-3.527697400000E+01	2.422001000000E+00
1758	4.044498800000E+01	-3.487411100000E+01	4.156886000000E+00
1759	4.044673500000E+01	-3.480372200000E+01	1.051946600000E+01
1761	4.045147300000E+01	-3.544971100000E+01	3.402515000000E+00
1763	4.045186600000E+01	-3.499679900000E+01	3.820982000000E+00
1764	4.045186600000E+01	-3.502629100000E+01	3.416038000000E+00
1770	4.046028500000E+01	-3.400060700000E+01	3.556368000000E+00
1774	4.046818900000E+01	-3.348350500000E+01	6.939595000000E+00
1781	4.048560300000E+01	-3.330033100000E+01	4.520063000000E+00
1784	4.048912000000E+01	-3.544909700000E+01	3.877169000000E+00
1785	4.049098600000E+01	-3.434756500000E+01	2.754435000000E+00
1786	4.049153100000E+01	-3.473661000000E+01	3.558995000000E+00
1787	4.049167300000E+01	-3.318814800000E+01	4.775496000000E+00
1789	4.050068700000E+01	-3.431510500000E+01	3.986428000000E+00
1794	4.051034500000E+01	-3.492783700000E+01	2.092262000000E+00
1795	4.051039100000E+01	-3.380703400000E+01	3.465362000000E+00
1802	4.052447500000E+01	-3.471269600000E+01	4.382675000000E+00
1803	4.052555100000E+01	-3.396065900000E+01	4.179580000000E+00
1805	4.052601600000E+01	-3.505670200000E+01	3.591199000000E+00
1806	4.052898800000E+01	-3.443558500000E+01	4.586955000000E+00
1808	4.053171500000E+01	-3.372229400000E+01	1.098599000000E+00
1810	4.053183000000E+01	-3.466552400000E+01	3.973668549020E+00
1819	4.054260300000E+01	-3.384105300000E+01	4.511580000000E+00
1820	4.054268300000E+01	-3.427143900000E+01	1.969713000000E+00
1821	4.054279300000E+01	-3.446903200000E+01	3.835005000000E+00
1824	4.054497100000E+01	-3.491154500000E+01	3.335855000000E+00
1828	4.054831700000E+01	-3.459750000000E+01	4.246135000000E+00
1829	4.054919400000E+01	-3.348459200000E+01	3.604901000000E+00
1832	4.055729300000E+01	-3.505195600000E+01	3.613899000000E+00
1834	4.056099700000E+01	-3.337079200000E+01	4.306791000000E+00
1835	4.056204600000E+01	-3.476715900000E+01	3.084007000000E+00
1836	4.056444900000E+01	-3.360057100000E+01	3.102457000000E+00
1837	4.056546800000E+01	-3.356010400000E+01	4.848845000000E+00
1839	4.056568100000E+01	-3.408392700000E+01	3.940617000000E+00
1842	4.056748600000E+01	-3.423003400000E+01	5.556517000000E+00
1843	4.057129700000E+01	-3.438574200000E+01	4.820735000000E+00
1844	4.057243700000E+01	-3.378619000000E+01	3.311943000000E+00
1846	4.057511500000E+01	-3.343330800000E+01	4.366086000000E+00
1849	4.058432400000E+01	-3.435129200000E+01	4.029622000000E+00
1855	4.058771500000E+01	-3.321348200000E+01	6.037169000000E+00

1856	4.058908100000E+01	-3.499603300000E+01	4.423262000000E+00
1863	4.060557600000E+01	-3.398458100000E+01	3.239489000000E+00
1866	4.060837600000E+01	-3.320393400000E+01	3.100695000000E+00
1869	4.061465800000E+01	-3.456669600000E+01	4.993159000000E+00
1872	4.062453500000E+01	-3.349603700000E+01	2.455181000000E+00
1873	4.062540400000E+01	-3.358249700000E+01	3.191709000000E+00
1874	4.062562900000E+01	-3.338298800000E+01	4.579771000000E+00
1875	4.062739900000E+01	-3.361782100000E+01	4.879014000000E+00
1876	4.063039000000E+01	-3.343563800000E+01	3.055478000000E+00
1877	4.063155700000E+01	-3.422454800000E+01	3.203215000000E+00
1882	4.064293700000E+01	-3.346781500000E+01	8.324242000000E+00
1883	4.064363500000E+01	-3.500733600000E+01	5.226137000000E+00
1885	4.064753000000E+01	-3.328094100000E+01	5.164039000000E+00
1887	4.065361400000E+01	-3.430286000000E+01	4.263285000000E+00
1888	4.065403700000E+01	-3.342842100000E+01	2.246765000000E+00
1893	4.066299100000E+01	-3.441542100000E+01	2.077250000000E+00
1895	4.066440200000E+01	-3.527265900000E+01	3.930020000000E+00
1907	4.068376500000E+01	-3.500577200000E+01	3.680984000000E+00
1909	4.068610400000E+01	-3.384361600000E+01	3.774800000000E+00
1920	4.071038800000E+01	-3.466247200000E+01	2.582696000000E+00
1923	4.071680100000E+01	-3.455651900000E+01	3.223477000000E+00
1925	4.072705500000E+01	-3.343508900000E+01	3.106577000000E+00
1926	4.072714200000E+01	-3.489970400000E+01	5.828116000000E+00
1927	4.072914500000E+01	-3.432675600000E+01	4.524391000000E+00
1937	4.075264400000E+01	-3.416454700000E+01	2.608209000000E+00
1945	4.077430300000E+01	-3.338802300000E+01	5.834752000000E+00
1955	4.081074100000E+01	-3.428430900000E+01	4.072212000000E+00
1957	4.081504100000E+01	-3.393541700000E+01	2.205818000000E+00
1958	4.081767700000E+01	-3.352721800000E+01	5.144611000000E+00
1968	4.084191500000E+01	-3.378180700000E+01	3.381360000000E+00
1971	4.084681300000E+01	-3.499040200000E+01	3.530529000000E+00
1974	4.085305400000E+01	-3.434039700000E+01	5.369104000000E+00
1979	4.086393000000E+01	-3.407931500000E+01	2.096381000000E+00
1981	4.086658500000E+01	-3.461166400000E+01	4.723108000000E+00
1989	4.087802900000E+01	-3.369472100000E+01	4.679204000000E+00
1990	4.088470100000E+01	-3.473232700000E+01	1.876938000000E+00
1998	4.088929700000E+01	-3.432344100000E+01	3.351292000000E+00
2005	4.089955900000E+01	-3.384222400000E+01	4.361297000000E+00
2008	4.090268700000E+01	-3.351429000000E+01	5.424777000000E+00
2012	4.091406600000E+01	-3.386862600000E+01	1.049486300000E+01
2021	4.092305400000E+01	-3.460702100000E+01	2.862133000000E+00
2023	4.092857400000E+01	-3.388332000000E+01	2.050244000000E+00
2024	4.092869600000E+01	-3.413662300000E+01	2.582770000000E+00
2025	4.092886000000E+01	-3.477103800000E+01	4.370712000000E+00

2036	4.094671200000E+01	-3.496133800000E+01	4.400520000000E+00
2039	4.095158800000E+01	-3.425183900000E+01	4.233931000000E+00
2047	4.096236400000E+01	-3.397439600000E+01	2.445535000000E+00
2050	4.096509600000E+01	-3.490438100000E+01	3.995905000000E+00
2051	4.097112700000E+01	-3.472411700000E+01	4.221040000000E+00
2052	4.097377400000E+01	-3.362256200000E+01	6.385736000000E+00
2057	4.098070100000E+01	-3.428504600000E+01	5.251232000000E+00
2058	4.098109100000E+01	-3.367123800000E+01	3.830625000000E+00
2059	4.098186900000E+01	-3.397611600000E+01	4.532635000000E+00
2069	4.099652100000E+01	-3.446731200000E+01	3.187479000000E+00
2070	4.099762700000E+01	-3.473458900000E+01	3.568906000000E+00
2075	4.100563400000E+01	-3.418901800000E+01	4.166400000000E+00
2081	4.101509900000E+01	-3.432739300000E+01	4.749294000000E+00
2083	4.102298400000E+01	-3.387715100000E+01	2.914427000000E+00
2090	4.103273800000E+01	-3.447273300000E+01	2.496725000000E+00
2092	4.103325700000E+01	-3.466505400000E+01	4.490238000000E+00
2097	4.104077500000E+01	-3.428568600000E+01	4.784158000000E+00
2108	4.105857100000E+01	-3.451115800000E+01	4.621725000000E+00
2109	4.106087100000E+01	-3.434383400000E+01	4.192948000000E+00
2111	4.106454800000E+01	-3.442152400000E+01	3.021397000000E+00
2112	4.106502500000E+01	-3.440234800000E+01	3.594898000000E+00
2114	4.106658900000E+01	-3.429919100000E+01	3.504774000000E+00
2116	4.106998400000E+01	-3.475652300000E+01	5.552830000000E+00
2134	4.111089300000E+01	-3.461544400000E+01	4.140873000000E+00
2136	4.111141600000E+01	-3.364145300000E+01	6.111924000000E+00
2143	4.112031200000E+01	-3.465380100000E+01	5.034652000000E+00
2144	4.112101000000E+01	-3.438644000000E+01	3.726894000000E+00
2154	4.113156100000E+01	-3.402237700000E+01	4.273752000000E+00
2158	4.113606600000E+01	-3.447991900000E+01	2.735122000000E+00
2170	4.115470900000E+01	-3.379254500000E+01	3.275675000000E+00
2171	4.115483900000E+01	-3.415947000000E+01	3.612652000000E+00
2173	4.115991600000E+01	-3.385241300000E+01	3.676046000000E+00
2191	4.118214400000E+01	-3.407743100000E+01	3.390665000000E+00
2198	4.119755600000E+01	-3.421151400000E+01	4.735279000000E+00
2200	4.119921100000E+01	-3.401722700000E+01	1.668538000000E+00
2201	4.120008000000E+01	-3.392348500000E+01	4.031985000000E+00

Table 9: The filtered and astrometrically corrected source catalog analysed in the thesis.

6 Eigenständigkeitserklärung

Hiermit bestätige ich, dass die vorliegende Arbeit von mir selbst verfasst wurde, dabei nur die angegebenen Quellen und Hilfsmittel verwendet wurden und dass sie nicht in wesentlichen Teilen mit einer Arbeit übereinstimmt, die bereits einer anderen Prüfungsbehörde vorgelegt wurde.

Bamberg, 15.02.2023
Ort, Datum

Martin Reh